EUROPEAN ORGANIZATION FOR NUCLEAR RESEARCH

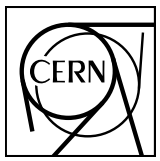

ALICE-PUBLIC-2014-001
July 2, 2014

Production of Υ(1S) at forward rapidity in Pb–Pb collisions at $\sqrt{s_{\rm NN}} = 2.76$ TeV

The ALICE Collaboration *

Abstract

The ALICE experiment has measured the Υ(1S) production in Pb–Pb collisions at $\sqrt{s_{\rm NN}} = 2.76$ TeV. The measurement is performed at forward rapidity ($2.5 < y < 4$) and down to zero transverse momentum via the dimuon decay channel. The Υ(1S) nuclear modification factor ($R_{\rm AA}$) is shown for two different collision centralities and in two rapidity intervals. Results are discussed and compared with the ALICE J/ψ measurements at forward rapidity, the mid-rapidity Υ(1S) data from the CMS Collaboration and theoretical predictions.

*See Appendix D for the list of collaboration members

Contents

1 Introduction

The primary aim of experiments with ultra-relativistic collisions of heavy nuclei (A–A) is to produce strongly-interacting matter at high temperature and pressure. Under such conditions Quantum Chromodynamics predicts the existence of a deconfined state of hadronic matter, the Quark-Gluon Plasma (QGP) [1–3]. Among the possible probes of the QGP, heavy quarks are of particular interest since they are produced in the primary partonic scatterings and coexist with the surrounding medium. Therefore, the measurements of quarkonia (charmonia and bottomonia) are expected to provide essential information on the properties of the QGP. In particular, according to the colour-screening model [4], the measurement of the in-medium dissociation probability of the various quarkonium states is expected to provide an estimate of the initial temperature of the system. Further details on heavy quarkonia can be found in a recent review [5].

Extensive experimental results in A–A collisions at SPS [6, 7] and at RHIC [8–10] show a significant suppression of the inclusive J/ψ yield with respect to expectation from pp collisions and scaling with the number of binary nucleon-nucleon collisions. At the energies reached at the LHC, the J/ψ production could be enhanced. Such an enhancement was first predicted if all J/ψ are generated at the phase boundary by statistical hadronisation [11, 12]. The recombination of deconfined c and $\overline{\mathrm{c}}$ quarks in the medium [13–15] is also expected to lead to quarkonium regeneration and possibly to an increase of the J/ψ yield. The nuclear modification factor of inclusive J/ψ, recently measured by the ALICE Collaboration [16, 17] at forward rapidity, shows a smaller suppression and a weaker centrality dependence at low transverse momentum compared with RHIC results. ALICE data are fairly described by both the statistical hadronisation model and the transport models including suppression and regeneration of J/ψ [16].

In A–A collisions, the Υ(1S) state is expected to dissociate at a much higher temperature than all the other bottomonium or charmonium states. The comparison of Υ(1S) production in A–A collisions with that of the other quarkonium states might therefore provide information on the QGP temperature [18]. In addition, the $\mathrm{b\overline{b}}$ production cross-section is smaller than that of $c\overline{c}$, resulting in a lower probability of production by recombination for bottomonium compared with charmonium. The CMS Collaboration has measured the production of Υ(1S), Υ(2S) and Υ(3S) states at mid-rapidity in Pb–Pb collisions at $\sqrt{s_{\mathrm{NN}}} = 2.76$ TeV [19, 20]. The results of the measurement are compatible with a sequential suppression of bottomonia.

Initial state effects, like modifications of the parton distribution functions in the nucleus relative to the nucleon (or shadowing), are also expected to be sizeable in A–A collisions at LHC energies. It is then necessary to disentangle the suppression due to the QGP from that due to such effects. These ones can be measured in proton-nucleus collisions (p–A) where the QGP is not expected to be formed.

In the ALICE experiment quarkonium production can be measured at forward rapidity ($2.5 < y < 4$) and down to zero transverse momentum, $p_{\mathrm{T}} > 0$, with the muon spectrometer. We present the measurement of the inclusive Υ(1S) nuclear modification factor in Pb–Pb collisions at $\sqrt{s_{\mathrm{NN}}} = 2.76$ TeV. Results will be compared with the ALICE inclusive J/ψ data [17] in the same kinematic interval and to the inclusive Υ(1S) data from the CMS Collaboration [20] in the $|y| < 2.4$ rapidity range. In addition, our data will be compared with the predictions of three models [21–23].

2 Experimental apparatus

In this section we describe briefly the experimental apparatus used in this analysis. More details on the ALICE detector can be found in [24]. The muon spectrometer, located at forward pseudo-rapidity

$(-4 < \eta < -2.5)$[1], consists of a ten interaction length thick front absorber filtering the muons upstream of five tracking stations comprising two planes of cathode pad chambers each. A dipole magnet with a 3 T·m field integral is used to bend the trajectory of charged particles passing through the tracking system. The detector is completed by a triggering system made of four planes of resistive plate chambers downstream of a 1.2 m thick iron wall. The iron wall stops efficiently the light hadrons which escape from the front absorber and a part of the low momentum muons coming mainly from π and K decays. Both tracking chambers and trigger chambers are protected by an absorber placed around the beam line and stretching along the whole detector length.

In this analysis, the V0 detector is used for trigger purposes and centrality estimates. The V0 is made of two arrays of 32 scintillator tiles which cover the full azimuth and the pseudo-rapidity ranges $2.8 < \eta < 5.1$ (V0-A) and a $-3.7 < \eta < -1.7$ (V0-C), respectively. The Zero Degree Calorimeters (ZDC), which are located at 114 meters upstream and downstream of the ALICE interaction point, are used to reject electromagnetic interactions. Finally, the Silicon Pixel Detector (SPD) is used to reconstruct the interaction vertex. This detector consists of two cylindrical layers covering the full azimuth and the pseudo-rapidity ranges $|\eta| < 2.0$ and $|\eta| < 1.4$ for the inner and outer layers, respectively.

3 Data Analysis

3.1 Data selection

The minimum bias (MB) trigger is defined as the coincidence of a signal in both the V0-A and the V0-C detectors synchronized with the passage of two colliding lead bunches. This MB trigger provides high trigger efficiency ($> 95\%$) for hadronic interactions. An additional threshold on the energy deposited in the ZDCs is used to reject the contribution from electromagnetic processes. The MB trigger was considerably down-scaled to open the DAQ bandwidth for more rare triggers. In particular, the unlike sign dimuon low-p_{T} trigger (p_{T} threshold[2] about 1 GeV/c), also called MUL, was used in this analysis. It is defined as the coincidence of the MB trigger requirements with the detection of two opposite-sign muons with a transverse momentum above the 1 GeV/c threshold. Beam-induced background was further reduced at the offline level by timing cuts on the signals from the V0 and from the ZDC.

A data sample of 17.3×10^6 Pb–Pb collisions triggered with the MUL condition was analysed. The equivalent number of MB events was obtained by multiplying the number of triggered events by an enhancement factor, F_{norm}, which corresponds to the inverse of the probability of having the MUL trigger condition verified in an MB event. The averaged value of F_{norm} over the data-taking period is $27.5 \pm 1.0(\mathrm{syst})$, where the systematic uncertainty reflects the spread of its values observed in different periods. Assuming a nuclear Pb–Pb cross-section $\sigma_{\mathrm{Pb-Pb}} = 7.7 \pm 0.1(\mathrm{stat})^{+0.6}_{-0.5}(\mathrm{syst})\mathrm{b}$ [25], the data sample corresponds to an integrated luminosity $L_{\mathrm{int}} = 68.8 \pm 0.9(\mathrm{stat}) \pm 2.5(\mathrm{syst\ F_{norm}})^{+5.5}_{-4.5}(\mathrm{syst})\ \mu\mathrm{b}^{-1}$.

Events were classified according to their centrality by means of the V0 detector amplitude, which was fitted using a Glauber model [26]. The centrality classes are defined as intervals in percentages of the hadronic Pb–Pb cross-section. With the Glauber model, it is also possible to estimate the variables related to the collision geometry, such as the average number of participant nucleons, $\langle N_{\mathrm{part}} \rangle$, the average number of binary collisions, $\langle N_{\mathrm{coll}} \rangle$, and the nuclear overlap function, $\langle T_{\mathrm{AA}} \rangle$, per centrality class. The $\langle T_{\mathrm{AA}} \rangle$ factor is equal to the average number of binary collisions divided by the inelastic nucleon-nucleon cross-section and can be interpreted as the nucleon-nucleon equivalent integrated luminosity per heavy-ion collision at a given event centrality [27].

[1] In the ALICE reference frame, the positive z-direction is along the counter clockwise beam direction. Thus, the muon spectrometer covers a negative pseudo-rapidity (η) range and a negative y range. In this note the results will be presented with a positive y notation keeping the η values signed.

[2] The threshold is defined as the p_{T} value where the trigger efficiency for single muons is 50%.

Events in the centrality interval 0-90% were used in this analysis. In this particular centrality range, the efficiency of the MB trigger is about 99% and the contribution of the electromagnetic background is negligible [26].

The data sample was divided in two centrality classes: 0–20% (central collisions) and 20–90% (semi-peripheral collisions). The corresponding numerical values for $\langle N_{\rm coll}\rangle$, $\langle N_{\rm part}\rangle$ and $\langle T_{\rm AA}\rangle$ are reported in Table 1.

Centrality	$\langle N_{\rm coll}\rangle$	$\langle N_{\rm part}\rangle$	$\langle T_{\rm AA}\rangle$ (mb^{-1})
0–90%	401±41	124±2	6.3±0.2
0–20%	1211±130	308±5	18.9±0.6
20–90%	170±16	72±3	2.7±0.1

Table 1: Average number of binary collisions, average number of participant nucleons and nuclear overlap function for the various centrality classes considered in this analysis [28].

3.2 Track selection

The high combinatorial background in Pb–Pb collisions reduces the signal significance and the signal-over-background ratio and imposes the following tight selection criteria on single muon tracks.

- The tracks with pseudo-rapidity in the acceptance of the spectrometer ($-4 < \eta < -2.5$) were selected.
- Each track reconstructed in the tracking chambers should match a track segment in the trigger chambers. This selection takes advantage of the iron wall of the muon spectrometer to reject light hadrons.
- Tracks crossing the part of the front absorber with the highest density material were rejected by a cut on their transverse radial coordinate at the end of the absorber[3] ($17.6 < R_{\rm ABS} < 89.5$ cm). This cut limits the impact of multiple scattering and energy loss effects, which degrade the invariant mass resolution.
- Tracks have to point to the interaction vertex. This selection is based on the correlation between momentum and Distance of Closest Approach[4] and significantly reduces the amount of fake and beam-induced tracks contaminating the muon sample.
- The transverse momentum of the tracks was required to be larger than 2 GeV/c. It was verified that this selection does not reduce signal counts, but reduces the background by about 20% in the Υ(1S) invariant mass range. This feature can be understood considering that muons from Υ(1S) decay have generally large $p_{\rm T}$ because of the large mass of the meson.

3.3 Signal extraction

The Υ(1S) candidates were formed by combining pairs of opposite-sign tracks with a rapidity in $2.5 < y < 4$. The signal extraction is based on the fit of the opposite-sign dimuon invariant mass distributions. The sum of the following five functions was considered as the default option (other choices are described later in this section).

[3] The end of the absorber is located at a longitudinal position $z = 5.1$ m after the interaction point.

[4] Distance between the extrapolated muon track and the interaction vertex, in the plane perpendicular to the beam direction and containing the vertex.

– The line shape of the Υ states is described by three Extended Crystal Ball (CB2) functions. The CB2 function consists of a Gaussian core with a power-law tail on both sides. It reproduces well the Υ(1S) distribution observed in MC simulations (section 4) and, in particular, the low invariant mass tail due to the muon energy loss in the front absorber and the high invariant mass one due to alignment and calibration biases. The expression of the CB2 can be found in Appendix A.

– The underlying continuum is described by a sum of two exponential functions (Double Exponential, or DE in the following). Simulations show that the main contribution to the dimuon continuum at high invariant mass comes from the semimuonic decays of D and B hadrons [29]. The DE allows us to satisfactorily reproduce the mass shape of this background.

The amplitude, the position and the width of the Υ(1S) were left free. The parameters of the DE and the amplitude of the Υ(2S) and the Υ(3S) were left free as well. Because of the few entries observed for invariant masses above ~ 9.8 GeV/c^2, the width and the position of the Υ(2S) and Υ(3S) were constrained. The mass differences between states were fixed from the PDG values [30] and the width for the Υ(2S) and Υ(3S) were forced to scale proportionally with that of the Υ(1S) according to the PDG mass ratio. Besides, since signal distribution tails are poorly constrained by the data, the tail parameters of the CB2 were fixed according to the results from MC simulations (section 4).

The fit procedure was applied to the invariant mass distribution for various centrality and rapidity ranges (Fig. 1). The Signal-over-background ratio, the significance, the peak position and the width for the Υ(1S) state are summarised in Table 2. The position of the Υ(1S) peak is globally consistent with the PDG meson mass (9.460 GeV/c^2) [30]. The signal-over-background ratio (S/B) is always larger than unity and the significance ($\frac{S}{\sqrt{S+B}}$) is always larger than 5. The S/B ratio and the significance were evaluated at 3σ. Namely, the number of signal and background counts were obtained in an invariant mass range centred on the Υ(1S) peak position and covering ± 3 times its width.

Centrality	Rapidity	S/B	Significance	Mass (GeV/c^2)	Width (MeV/c^2)
0–90%	$2.5< y <4$	1.3 ± 0.2	8 ± 1	9.44 ± 0.03	144 ± 27
0–20%		1.0 ± 0.2	5 ± 1	9.44 ± 0.04	136 ± 40
20–90%		1.8 ± 0.4	6 ± 1	9.46 ± 0.04	150 ± 37
0–90%	$2.5< y <3.2$	1.6 ± 0.3	6 ± 1	9.49 ± 0.03	107 ± 25
	$3.2< y <4$	1.1 ± 0.2	5 ± 1	9.34 ± 0.05	159 ± 40

Table 2: Signal-over-background ratio, significance, peak position and width for the Υ(1S) state obtained applying the default fit procedure. The statistical uncertainties are also mentioned. Values are reported for the different centrality classes and the different rapidity ranges considered in the analysis. Signal-over-background ratio and significance were evaluated in the interval $\pm 3\sigma$.

Centrality	Rapidity	Counts $N \pm$stat$\pm$syst
0–90%	$2.5< y <4$	$134 \pm 20 \pm 7$
0–20%		$64 \pm 14 \pm 4$
20–90%		$66 \pm 12 \pm 4$
0–90%	$2.5< y <3.2$	$72 \pm 13 \pm 4$
	$3.2< y <4$	$57 \pm 13 \pm 6$

Table 3: Signal extraction results. The obtained number of Υ(1S) is quoted with the related statistical and systematic uncertainties.

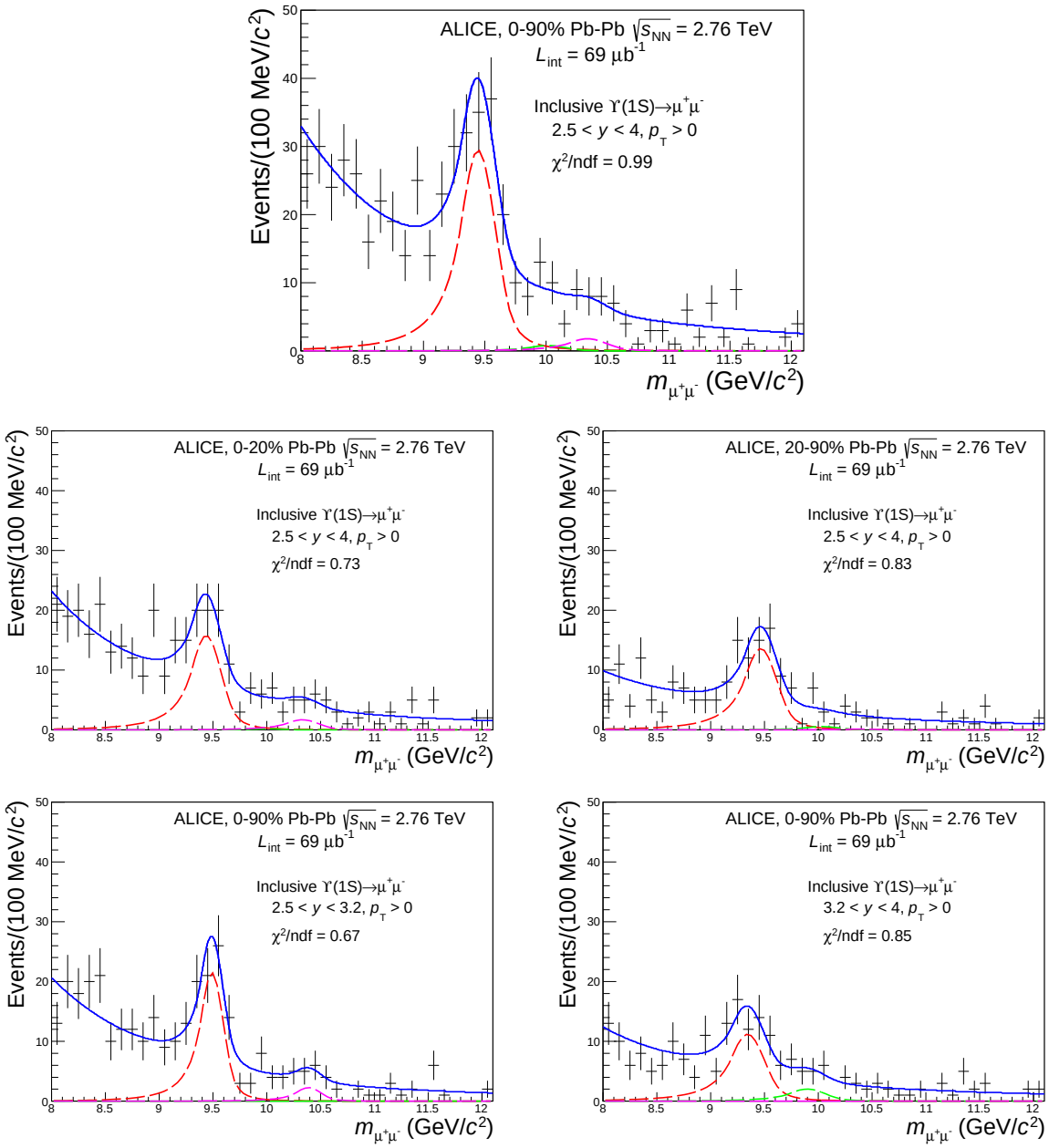

Fig. 1: Default fit procedure applied to the invariant mass distributions of opposite-sign dimuons in different centrality and rapidity intervals. The total fit function is represented by the full line. The dashed lines represent the CB2 for ϒ states. The χ^2 per degree of freedom (χ^2/ndf) is also shown.

Variations of the fit method were performed to estimate the systematic uncertainties on the number of signal counts. Only fits with a χ^2/ndf smaller than 1.5 were considered and it was checked that the $\Upsilon(1S)$ peak width and position were constant within uncertainties.

In addition to the DE function a Double Power-Law (DPL) function, defined as the sum of two power-law functions, was used to describe the underlying background. For each function, the lower and the upper bounds of the fit range were independently modified within the limits where the background is reasonably fitted. The DPL function leads to fits with higher χ^2/ndf than the DE. Nevertheless almost all the fits have a χ^2/ndf below the 1.5 threshold and we cannot discard the possibility of a DPL shaped background. The systematic uncertainty resulting from this study ranges between 2% and 5% depending on the considered rapidity or centrality interval.

The position and the width of the $\Upsilon(2S)$ and the $\Upsilon(3S)$ resonances were independently shifted by different values. These values were chosen in an interval corresponding to the statistical uncertainty on the $\Upsilon(1S)$ position and width provided by the fit (about 5‰ for the position and 20% for the width). The resulting uncertainty is of the order of 1%.

The CB2 tail parameters for the Υ states were varied according to the uncertainties in their determination from fits of the MC signal distributions. parameters were first modified by the same quantity for each state, then the variation was done independently. The overall systematic uncertainty ranges from 1% to 3% depending on the considered centrality or rapidity range.

Table 3 reports the values from the signal extraction. Central values and statistical uncertainties are the average of the results obtained for each study. Systematic uncertainties from each source were summed in quadrature. Overall statistical (systematic) uncertainties range between 15% and 22% (5% and 10%).

4 Acceptance and efficiency corrections

4.1 Results from embedding production

The embedding MC method consists in simulating a signal particle (a $\Upsilon(1S)$ in our case) and embedding the corresponding hits generated in the detector inside those of a real raw data event. This method reproduces the detector response to the signal in a highly realistic background environment and accounts for possible variations of the reconstruction efficiency with the collision centrality. The $\Upsilon(1S)$ were generated according to realistic parametrisations of their p_{T} and y distributions [31] and were forced to decay into dimuons. The detector response was provided by GEANT3 [32] taking into account the time dependence of the detector efficiency and the residual misalignment of the tracking chambers. The efficiency of the muon trigger and tracking systems was calculated from data and is based on the analysis of the hit distributions in the different planes of the detection chambers [33].

The product of acceptance times efficiency ($A \times \varepsilon$) is defined as the probability for the decay muons from $\Upsilon(1S)$ produced in the geometrical acceptance of the detector to be correctly reconstructed and identified, taking into account the efficiency of the tracking and triggering systems.

The average $A \times \varepsilon$ obtained from the embedding simulations is $21.9 \pm 0.1(\mathrm{stat})\%$. Fig. 2 (left) shows the $A \times \varepsilon$ as a function of centrality. From peripheral (80–90%) to central collisions (0–10%), we observe a 7% decrease explained by the efficiency loss with increasing tracking chamber occupancy. Fig. 2 (right) shows the $A \times \varepsilon$ as a function of rapidity. The latter is maximal at the centre of the detector and decreases at the edges. This effect is purely geometrical and reflects the detector acceptance. The results for each rapidity and centrality interval considered further in the analysis are summarised in Table 4.

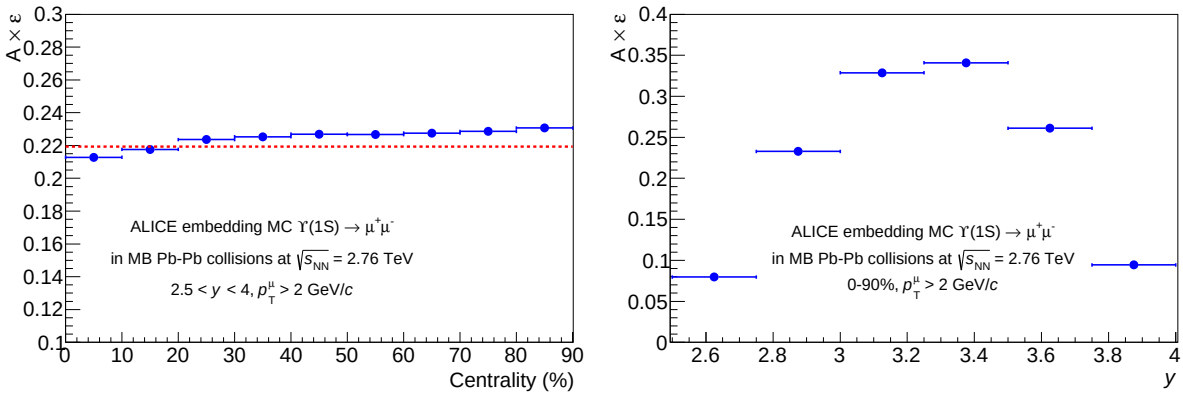

Fig. 2: Left: $A \times \varepsilon$ as a function of centrality. The red dotted line represents the mean value. Right: $A \times \varepsilon$ as a function of rapidity.

Centrality	Rapidity	$A \times \varepsilon$ (%) Value$\pm$stat
0–90%	$2.5 < y < 4$	21.9 ± 0.1
0–20%		21.6 ± 0.1
20–90%		22.6 ± 0.1
0–90%	$2.5 < y < 3.2$	19.3 ± 0.1
	$3.2 < y < 4$	25.7 ± 0.1

Table 4: $A \times \varepsilon$ values for the intervals considered in this analysis.

4.2 Systematic uncertainties

The estimate of $A \times \varepsilon$ depends on the Υ(1S) $p_{\rm T}$ and y shapes used as input distributions in the MC simulations. In order to evaluate the sensitivity of the results to this choice, several $A \times \varepsilon$ calculations were performed with significantly different $p_{\rm T}$ and y parametrisations [31] corresponding to different systems, energies and centralities. The input distributions were chosen different enough to include the a priori unknown nuclear matter effects. The maximum spread observed among the obtained $A \times \varepsilon$ values varies between 4% and 7% (in relative) depending on the considered rapidity range. These values are used as systematic uncertainties.

The systematic uncertainty on the efficiency of track reconstruction was estimated by comparing the results from simulations with those obtained from data. In both cases, the efficiency was evaluated with an algorithm [33] based on the analysis of hit distributions in the tracking chambers. The systematic uncertainty was determined at the single muon level and was properly combined according to the kinematic distributions of decay muons from Υ(1S) to obtain the uncertainty at the dimuon level. This one is 8% for the two centrality ranges under study, while it is 7% (9%) for the $2.5 < y < 3.2$ ($3.2 < y < 4$) interval. Another uncertainty arises from restricted inactive areas on the various chambers, covering the same geometric acceptance. Their presence affects the algorithm used to determine the tracking efficiency, giving an extra 2% systematic uncertainty. This uncertainty is not fully uncorrelated with the previous one and has to be added to the total uncertainty for both y-integrated and centrality-integrated results.

A systematic uncertainty of 2% on the trigger efficiency was estimated from the comparison of MC results obtained with different chamber efficiency maps. The maps were obtained from data for various detector occupancies and particle transverse momenta[5].

[5]The algorithmic extrapolation of the track from the tracker to the trigger is more accurate with increasing transverse momentum, thus leading to an effect to be considered.

In addition, a systematic uncertainty of 1% on the matching of the trigger and tracking information was considered. In order to estimate this value, the matching efficiency obtained from data with different cuts on the χ^2 of the matching was compared with simulation results obtained in the same conditions.

An overall effect of 1% accounts for the tracking, trigger and matching systematic uncertainties dependence on the centrality. This effect is largely dominated by the systematic on tracking efficiency. It was estimated by comparing the efficiency obtained with the embedding MC simulation to the one obtained from data.

Since available data favour a small or null polarization for Υ(1S) [34–36], an unpolarised production was assumed in Pb–Pb and no polarisation uncertainty was assigned to $A \times \varepsilon$.

A summary of uncertainties on acceptance and efficiency is reported in Table 5.

	MC input distributions	Tracking	Trigger	Matching
0–90%	4	10	2	1
0–20%	4	10	2	1
20–90%	4	10	2	1
$2.5 < y < 3.2$	7	9	2	1
$3.2 < y < 4$	5	11	2	1

Table 5: Summary of systematic uncertainties on acceptance and efficiency (%).

5 Proton-proton reference cross-section

A reference cross-section in pp collisions at $\sqrt{s} = 2.76$ TeV and in the $2.5 < y < 4$ rapidity region is needed for the $R_{\rm AA}$ calculation (section 6). Due to the limited number of events collected in pp collisions at $\sqrt{s} = 2.76$ TeV, ALICE did not measure $\sigma^{\rm pp}_{\Upsilon(1S)}$. The LHCb data [37] were used to define the reference. The LHCb measurement was carried out in 6 rapidity intervals in $2 < y < 4.5$. A summary of the results provided by LHCb is given in Table 6.

Rapidity	BR$\times\sigma^{\rm pp}_{\Upsilon(1S)} \pm$ stat $\pm$ syst (nb)
$2.5 < y < 4$	$0.670 \pm 0.025 \pm 0.026$
$2 < y < 2.5$	$0.404 \pm 0.034 \pm 0.022$
$2.5 < y < 3$	$0.321 \pm 0.018 \pm 0.012$
$3 < y < 3.5$	$0.227 \pm 0.013 \pm 0.008$
$3.5 < y < 4$	$0.124 \pm 0.011 \pm 0.005$
$4 < y < 4.5$	$0.035 \pm 0.008 \pm 0.002$

Table 6: Inclusive Υ(1S) cross-section in pp collisions at $\sqrt{s} = 2.76$ TeV provided by LHCb [37] in different rapidity intervals. The results are multiplied by BR, the branching ratio of Υ(1S) to dimuon (BR $=2.48\pm0.05\%$) [30].

The y-differential cross-section of $\Upsilon(1S) \to \mu^+\mu^-$ is shown in Fig. 3. It was obtained by dividing the values reported in Table 6 by the bin width. For each rapidity range, statistical and systematic uncertainties were summed in quadrature. LHCb systematic uncertainties are reported to be strongly correlated with rapidity but the degree of correlation is not provided. As an educated guess we have chosen to consider the minimum relative systematic uncertainty quoted for the various rapidity intervals (Table 6) as fully correlated. Under this assumption the results obtained by integrating the LHCb y-differential cross-section are similar to the total cross-section [37]. The correlated uncertainty was subtracted quadratically from the data shown in Fig. 3. It is then considered as correlated uncertainty in our final results (Table 7).

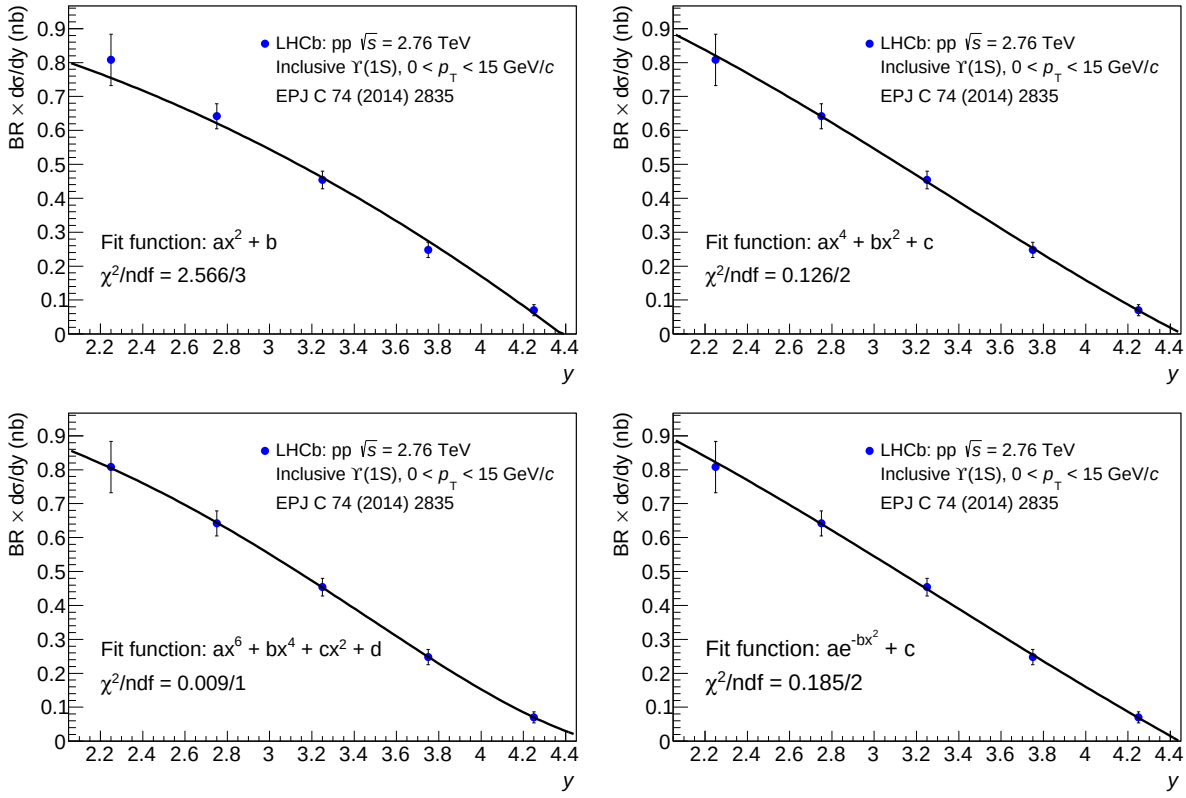

Fig. 3: Rapidity differential cross-section of $\Upsilon(1S) \to \mu^+\mu^-$ obtained from LHCb data [37] as explained in the text. Results are fitted with different functions. The χ^2 divided by the number of free parameters is also shown.

The y-differential cross-section was fitted with various functions symmetric with respect to $y = 0$ and having a number of free parameters between 1 and 3. The fit results and the corresponding χ^2 per degree of freedom are shown in Fig. 3. The four considered functions reproduce well the data and the χ^2 per degree of freedom remains smaller than 1.

The functions were integrated over the required rapidity ranges and, for each range, the fit results were averaged. Uncorrelated systematic uncertainties were obtained by summing in quadrature the largest fit uncertainty and the half spread of the different results obtained with the different fitting functions. Results in the $2.5 < y < 3.2$ and $3.2 < y < 4$ rapidity ranges are given it Table 7.

Rapidity	$\sigma^{pp}_{\Upsilon(1S)} \pm$ uncorr $\pm$ corr (nb)
$2.5 < y < 3.2$	$16.93 \pm 0.73 \pm 0.60$
$3.2 < y < 4$	$10.20 \pm 0.64 \pm 0.36$

Table 7: Inclusive Υ(1S) cross-section in pp collisions at $\sqrt{s} = 2.76$ TeV obtained from the rapidity interpolation of LHCb data [37]. Uncorrelated systematic uncertainties are quoted as uncorr and correlated systematic uncertainties as corr. Results do not include the branching ratio of Υ(1S) decay to dimuon.

When ALICE preliminary results [38] were released, the LHCb data were not yet available and $\sigma^{pp}_{\Upsilon(1S)}$ was estimated using a data-driven method as explained in Appendix B. Depending on the rapidity interval, the pp reference obtained with this approach and the LHCb data [37] differ by 30-35%. Taking into account uncertainties, it implies a change on the modification factor (see section 6.2) by 1.3 to 2.2σ, depending on rapidity.

6 Results

6.1 Production yields in Pb–Pb collisions

The yield of inclusive Υ(1S) is estimated from the number of signal counts (section 3.3), $N_{\Upsilon(1S)}$, the number of MB Pb–Pb events (section 3.1), $N_{\rm MB}$, the acceptance and efficiency correction factor (section 4.1), $A \times \varepsilon$ and the $\Upsilon(1S) \to \mu^+\mu^-$ branching ratio (BR =2.48$\pm$0.05%) [30]:

$$Y_{\Upsilon(1S)} = \frac{N_{\Upsilon(1S)}}{BR \cdot N_{\rm MB} \cdot A \times \varepsilon}. \quad (1)$$

Since the distribution of the number of MB events is by definition flat with centrality, $N_{\rm MB}$ scales with the width of the considered centrality interval. The total equivalent number of MB events is obtained from the measured number of MUL events as explained in section 3.1.

Centrality	Rapidity	Yields $\times 10^5$ $Y \pm$stat $\pm$ uncorr $\pm$ corr
0–20%	$2.5 < y < 4$	$11.3 \pm 2.5 \pm 0.7 \pm 1.3$
20–90%		$3.2 \pm 0.6 \pm 0.2 \pm 0.4$
0–90%	$2.5 < y < 3.2$	$3.2 \pm 0.6 \pm 0.4 \pm 0.1$
	$3.2 < y < 4$	$1.9 \pm 0.4 \pm 0.3 \pm 0.1$

Table 8: Υ(1S) yields obtained in Pb–Pb collisions at $\sqrt{s_{\rm NN}} = 2.76$ TeV for each centrality and rapidity range. Uncorrelated (correlated) systematic uncertainties are quoted as uncorr (corr). When results are integrated on rapidity (centrality), the degree of correlation is mentioned with respect to centrality (rapidity).

The yield measured in the rapidity interval 0–90% and the rapidity range $2.5 < y < 4$ is $(5.2 \pm 0.8({\rm stat}) \pm 0.7({\rm syst})) \times 10^{-5}$. The values for the other centrality and rapidity ranges considered in the analysis

are reported in Table 8. The statistical uncertainties (stat), the uncorrelated systematic uncertainties (uncorr) and the correlated systematic uncertainties (corr) were obtained by summing in quadrature the contribution from each term of Eq. 1. It has to be mentioned that the systematic uncertainties on $A \times \varepsilon$ are fully correlated with centrality and uncorrelated with rapidity. Therefore, the correlated uncertainty for y-integrated results is larger than for centrality-integrated ones. See section 6.2.1 for a list of uncorrelated and correlated systematic uncertainties.

6.2 Nuclear modification factor

The Υ(1S) nuclear modification factor, $R_{\rm AA}$, was obtained by dividing the corresponding yield (equation 1) by $\langle T_{\rm AA} \rangle$, the average nuclear overlap function (section 3.1) and by $\sigma^{pp}_{\Upsilon(1S)}$, the pp reference cross-section (section 5):

$$R_{\rm AA} = \frac{Y_{\Upsilon(1S)}}{\langle T_{\rm AA} \rangle \cdot \sigma^{pp}_{\Upsilon(1S)}}. \tag{2}$$

6.2.1 Summary of systematic uncertainties

The uncorrelated systematic uncertainties for the $R_{\rm AA}$ estimated as a function of centrality come from the signal extraction (section 3.3) and the nuclear overlap function (section 3.1). The correlated uncertainties arise from the pp reference cross-section (section 5), the estimate of the number of MB events (section 3.1) and the acceptance and efficiency correction (section 4.2).

The uncorrelated uncertainties for the $R_{\rm AA}$ as a function of rapidity come from the signal extraction and the efficiency correction. A part of the systematic uncertainties on the pp reference cross-section is also uncorrelated with rapidity. The correlated uncertainties are then the remaining part of the uncertainties on the pp reference cross-section, those on the number of MB events and those on the nuclear overlap function (in the 0–90% centrality range).

For both studies as a function of centrality and rapidity, the acceptance and efficiency correction is the largest contribution to the overall systematic uncertainty, followed by the uncertainty on the yield extraction. Quantitative information are summarised in Table 9.

	Signal extraction	$A \times \varepsilon$	$N_{\rm MB}$	$\langle T_{\rm AA} \rangle$	$\sigma_{\rm pp}$ (uncorrelated)	$\sigma_{\rm pp}$ (correlated)
0–90%	5	11	4	3	none	4
0–20%	7	11	4	3	none	4
20–90%	6	11	4	4	none	4
$2.5 < y < 3.2$	5	12	4	3	4	4
$3.2 < y < 4$	10	12	4	3	7	4

Table 9: Summary of systematic uncertainties (%).

6.2.2 Results

In 0–90% central events, the $R_{\rm AA}$ of inclusive Υ(1S) is $R_{\rm AA}^{0-90\%} = 0.30 \pm 0.05({\rm stat}) \pm 0.04({\rm syst})$, indicating a strong suppression.

The $R_{\rm AA}$ of inclusive Υ(1S) measured in the range $2.5 < y < 4$ and $p_{\rm T} > 0$ is shown in Fig. 4 (left) as a function of $\langle N_{\rm part} \rangle$. The statistical uncertainties dominate over the correlated systematic uncertainties and the uncorrelated systematic uncertainties. Since our centrality intervals are large, a horizontal error bar was assigned point-to-point. It corresponds to the Root Mean Square of the $N_{\rm part}$ distribution [26]. A suppression which increases with centrality is observed.

The $R_{\rm AA}$ of inclusive Υ(1S) integrated over centrality (0–90%) is shown in Fig. 4 (right) in two rapidity intervals ($2.5 < y < 3.2$ and $3.2 < y < 4$), for $p_{\rm T} > 0$. Statistical and uncorrelated uncertainties are almost the same, while they are much larger than correlated uncertainties. No clear rapidity dependence can be observed within the statistical and uncorrelated systematic uncertainties.

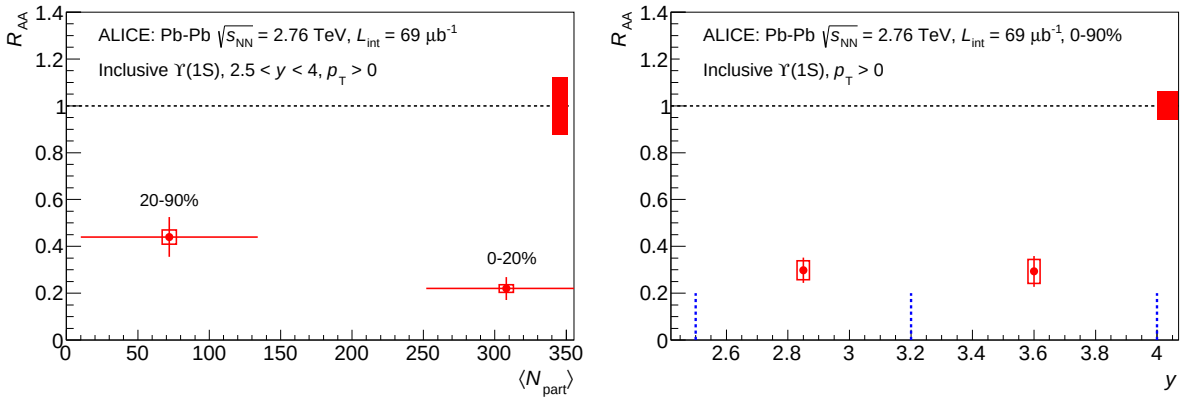

Fig. 4: Nuclear modification factor of the inclusive Υ(1S) as a function of the average number of participant nucleons (left) and as a function of rapidity (right). Vertical dotted lines on the right plot represent the rapidity bin widths. Bars stand for statistical uncertainties and boxes for uncorrelated systematic uncertainties. The correlated systematic uncertainty is shown as a box at $R_{\rm AA} = 1$. The point-to-point horizontal error bars on the left plot correspond to the Root Mean Square of the $N_{\rm part}$ distribution.

The $R_{\rm AA}$ values in the centrality and rapidity intervals considered in the analysis are summarised in Table 10. The details of systematic uncertainties are presented in section 6.2.1. Since our centrality ranges are large, the average number of participant nucleons weighted by the average number of binary collisions, $\langle N_{\rm part}^{\rm w} \rangle$, is also reported. The weighted average was calculated for each centrality class according to the values reported in [26] for narrow intervals. The $\langle N_{\rm part}^{\rm w} \rangle$ quantity represents a more precise evaluation of the average centrality for a given interval, since the Υ(1S) production is a hard process and its initial yield scales with the number of binary nucleon-nucleon collisions, in the absence of initial-state effects.

Centrality ($\langle N_{\rm part} \rangle$, $\langle N_{\rm part}^{\rm w} \rangle$)	Rapidity	$R_{\rm AA} \pm$ stat $\pm$ uncorr $\pm$ corr
0–20% (308, 323)	$2.5 < y < 4$	$0.22 \pm 0.05 \pm 0.02 \pm 0.03$
20–90% (72, 140)		$0.44 \pm 0.09 \pm 0.03 \pm 0.05$
0–90% (124, 262)	$2.5 < y < 3.2$	$0.30 \pm 0.05 \pm 0.04 \pm 0.02$
	$3.2 < y < 4$	$0.29 \pm 0.07 \pm 0.05 \pm 0.02$

Table 10: Values of the $R_{\rm AA}$ measured down to zero transverse momentum in Pb–Pb collisions at $\sqrt{s_{\rm NN}} = 2.76$ TeV. Statistical uncertainties are quoted as stat, uncorrelated systematic uncertainties are quoted as uncorr and correlated systematic uncertainties are quoted as corr

7 Discussion

7.1 Comparison with J/ψ ALICE measurements at forward rapidity

In Fig. 5 (left), the $R_{\rm AA}$ of inclusive Υ(1S) is compared with the ALICE $R_{\rm AA}$ of inclusive J/ψ [17] in the same kinematic range ($2.5 < y < 4$, $p_{\rm T} > 0$). The Υ(1S) suppression is larger than that of the J/ψ. In particular, the $R_{\rm AA}$ value is about two times larger for J/ψ than for Υ(1S) in central collisions while the results are closer for semi-peripheral ones. Fig. 5 (right) shows the ALICE Υ(1S) and J/ψ [17] $R_{\rm AA}$ as a function of rapidity. Both results are integrated over the 0–90% centrality range. Υ(1S) states are more

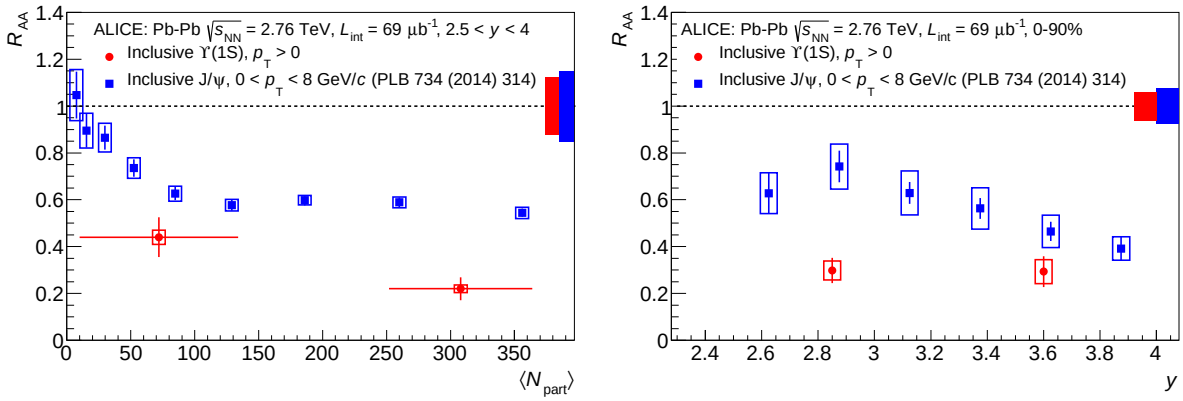

Fig. 5: Comparison of the ALICE nuclear modification factor of inclusive ϒ(1S) and J/ψ [17] in the same kinematic range. Left (Right): results are shown as a function of the average number of participant nucleons (rapidity). Bars stand for statistical uncertainties and boxes for uncorrelated systematic uncertainties. The correlated systematic uncertainty is shown as a box at $R_{AA} = 1$. The point-to-point horizontal error bars on the left plot correspond to the Root Mean Square of the N_{part} distribution.

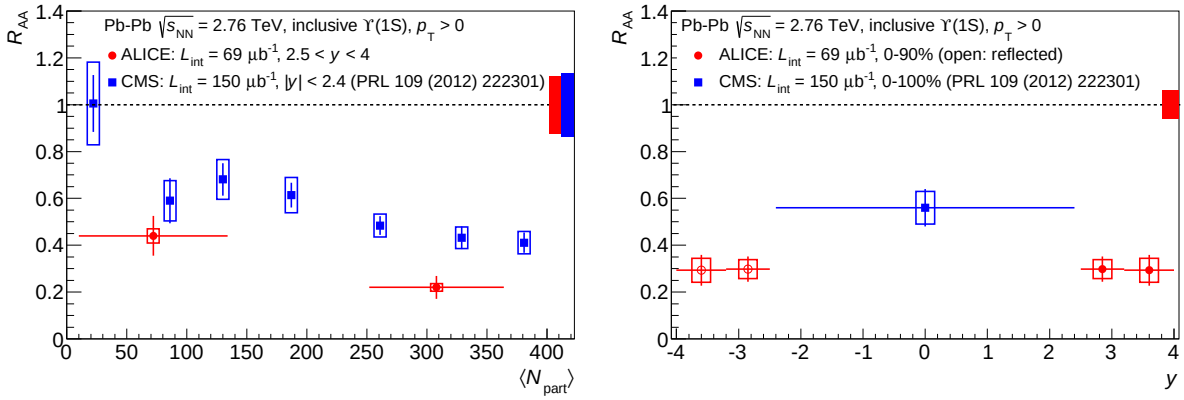

Fig. 6: Left (Right): ALICE and CMS [20] nuclear modification factor of inclusive ϒ(1S) production as a function of the average number of participant nucleons (rapidity). The same conventions as in Fig. 5 are used to show the uncertainties. On the right plot, open points are reflected with respect to the measured ones.

suppressed than J/ψ and the difference between the R_{AA} values is the largest in the $2.5 < y < 3.2$ rapidity range.

Comparisons between theory and data have suggested an important contribution of J/ψ (re-)generation in Pb–Pb collisions at $\sqrt{s_{NN}} = 2.76$ TeV [17], while in the ϒ(1S) case this contribution is expected to be much less important. Besides, the feed-down contribution from higher mass states to the ϒ(1S) is expected to be substantial and could be of the order of 40–50% [39–41]. These aspects have to be taken into account to interpret the different suppression features for the J/ψ and the ϒ(1S).

7.2 Comparison with ϒ(1S) measurements by the CMS Collaboration

The R_{AA} of inclusive ϒ(1S) measured in the $2.5 < y < 4$ rapidity range is compared with the CMS data in the range $|y| < 2.4$ [20]. Both ALICE and CMS experiments measure the ϒ(1S) state down to $p_T = 0$. The comparison of the R_{AA} as a function of the average number of participant nucleons is shown in Fig. 6 (left). In central collisions, the suppression is stronger at forward rapidity than at mid-rapidity.

R_{AA} as a function of rapidity are compared in Fig. 6 (right). The CMS and ALICE data are integrated over a similar centrality range (0–90% for ALICE and 0–100% for CMS). The value of the ϒ(1S) R_{AA}

in $2.5 < y < 4$ is significantly lower than in $|y| < 2.4$.

7.3 Comparison with theoretical predictions

7.3.1 Dynamical model

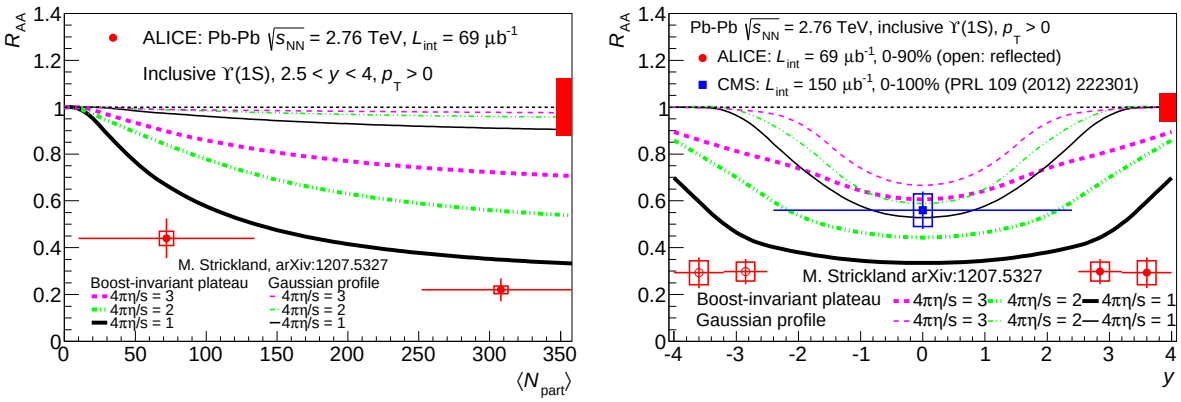

Fig. 7: Left (Right): ALICE $R_{\rm AA}$ of inclusive ϒ(1S) as a function of the average number of participant nucleons (rapidity) compared with theoretical predictions from [21]. The CMS data point at mid-rapidity is included in the rapidity plot. The same conventions as in Fig. 5 are used to show the uncertainties. On the right plot, open points are reflected with respect to the measured ones.

The observed ϒ(1S) nuclear modification factor is compared with the theoretical predictions by M. Strickland *et al.* [21, 42, 43]. The calculation of the bottomonium suppression is based on a complex-potential approach in an evolving QGP described by means of a hydrodynamical model. The model only includes the effects of in-medium suppression of bottomonium states. It does not include recombination or Cold Nuclear Matter (CNM) effects.

In Fig. 7 two sets of calculations are presented [21]. They correspond to different initial temperature profiles in rapidity. One case assumes a broad plateau containing a boost-invariant central rapidity region with half-Gaussian tails in the forward and backward directions. This profile is expected in the Bjorken picture of heavy-ion collisions [44]. The other case assumes a Gaussian profile which corresponds to the Landau picture [45]. Three values for the plasma shear-viscosity-to-entropy-density ratio were considered for each profile ($4\pi\eta/s = \{1,2,3\}$) and are depicted by the bottom, the middle and the top lines, respectively. None of the calculations reproduce the ALICE data and the observed suppression is underestimated in all cases. In particular, the $R_{\rm AA}$ rapidity dependence predicted in the wide range covered by ALICE and CMS is the opposite of the measured one. It has to be noted that, given our large centrality intervals, the observed suppression in semi-peripheral collisions is consistent with the model predictions when the minimum possible value of $4\pi\eta/$s ($4\pi\eta/\mathrm{s} = 1$) is adopted in the Bjorken scenario.

7.3.2 Transport models

The observed ϒ(1S) $R_{\rm AA}$ has also been compared with the theoretical predictions by A. Emerick *et al.* [22, 46]. This model includes a suppression and a small regeneration component which are implemented by means of a rate equation. An effective absorption cross-section ($\sigma_{\rm abs}$) is used to describe CNM effects including the effects of the nuclear modifications of parton distribution functions, the effects of the absorption in CNM and the parton intrinsic transverse momentum ($k_{\rm T}$) broadening.

In Fig. 8 the predictions are shown as a function of the number of participant nucleons (left). The $R_{\rm AA}$ of inclusive and primordial[6] ϒ(1S) are represented as bands obtained with two extreme values for $\sigma_{\rm abs}$

[6]Namely, the ϒ(1S) states created in the first stages of the Pb–Pb collisions and which have survived to the QGP formation or those coming from the feed-down from higher mass state.

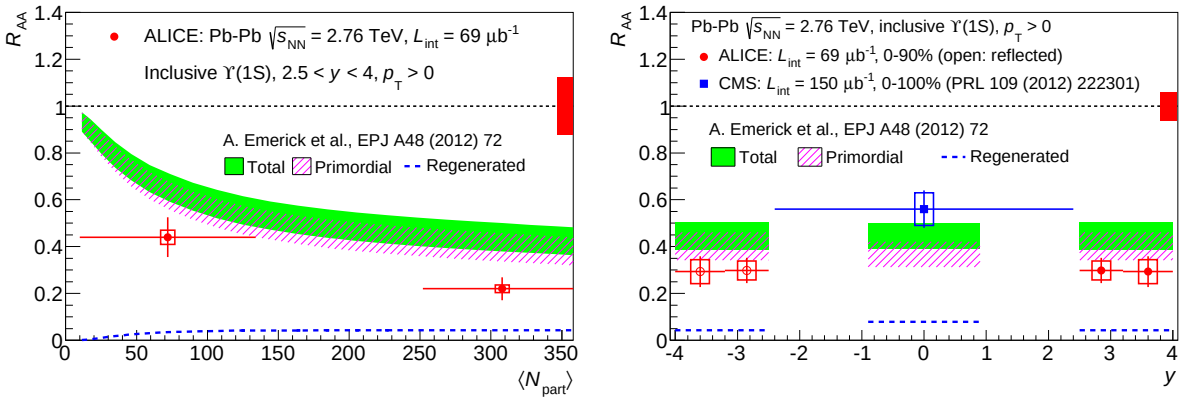

Fig. 8: ALICE nuclear modification factor of inclusive ϒ(1S) as a function of the average number of participant nucleons (left) and rapidity (right) compared with theoretical predictions from [22, 46]. The CMS data point at mid-rapidity is included in the rapidity plot. The same conventions as in Fig. 5 are used to show the uncertainties. On the right plot, open points are reflected with respect to the measured ones.

($\sigma_{abs} = 0$ mb and $\sigma_{abs} = 2.0$ mb). The contribution of regenerated ϒ(1S) is also shown. The primordial ϒ(1S) component dominates over the regeneration one. The measured R_{AA} is overestimated by the calculation which, however, reproduces the decreasing trend of the R_{AA}. In Fig. 8 (right), the predictions are compared with the ALICE and CMS data as a function of rapidity. The transport model predicts a R_{AA} which remains almost constant as a function of rapidity. This result is not supported by the data.

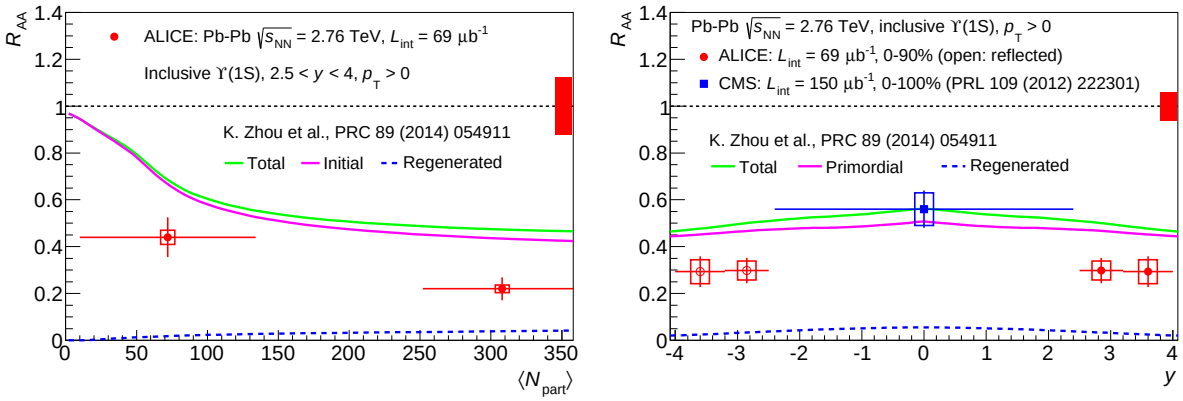

Fig. 9: ALICE nuclear modification factor of inclusive ϒ(1S) as a function of the average number of participant nucleons (left) and as a function of rapidity (right) compared with theoretical predictions from [23, 47]. The CMS data point at mid-rapidity is included in the rapidity plot. The same conventions as in Fig. 5 are used to show the uncertainties. On the right plot, open points are reflected with respect to the measured ones.

In Fig. 9, the ALICE R_{AA} is compared with the predictions of another transport model by Zhou *et al.* [23, 47]. This model includes a suppression and a small regeneration component while CNM effects are evaluated employing the EKS98 shadowing parametrization [48].

In Fig. 9 (left), the R_{AA} is shown as a function of centrality together with the predictions from [23, 47]. The model calculations underestimate the observed suppression but reproduce the centrality dependence of the data. In Fig. 9 (right), the ALICE and CMS R_{AA} are shown as a function of rapidity. The model reproduces well the CMS data but underestimates the strong suppression observed at forward rapidity and fails to reproduce its rapidity dependence. It has to be mentioned that, due to our large centrality ranges, the suppression observed in semi-peripheral collisions is compatible with the predictions of both transport models.

In the transport [22, 23, 46, 47] and the dynamical [22, 46] models the inclusive Υ(1S) suppression is mostly determined by the in-medium dissociation of higher mass bottomonia. The fact that both models overestimate the measured $R_{\rm AA}$ suggests that the suppression of direct Υ(1S) might be underestimated. However, the assumptions on the magnitude of CNM effects and on the contribution of the feed-down from higher mass bottomonia need to be verified and constrained by accurate pp and Pb–Pb data.

8 Conclusions

The inclusive Υ(1S) nuclear modification factor in Pb–Pb collisions at $\sqrt{s_{\rm NN}} = 2.76$ TeV has been measured down to $p_{\rm T} = 0$ in the $2.5 < y < 4$ rapidity and 0–90% centrality ranges. We obtained $R_{\rm AA}^{0-90\%} = 0.30 \pm 0.05({\rm stat}) \pm 0.04({\rm syst})$. The suppression is more pronounced in central collisions than in semi-peripheral ones. The $R_{\rm AA}$ was also measured in two rapidity intervals and, within uncertainties, no significant rapidity dependence was observed in the range covered by the ALICE muon spectrometer.

The data were compared with the ALICE J/ψ results in the same kinematic range. The Υ(1S) is more suppressed than the J/ψ and the difference of $R_{\rm AA}$ is particularly pronounced in the 0–20% ($2.5 < y < 3.2$) centrality (rapidity) range. The interpretation of these results is not straightforward due to the different sizes of the expected feed-down and (re-)generation effects for the two quarkonium states.

The Υ(1S) $R_{\rm AA}$ was also compared with CMS data measured in the $|y| < 2.4$ rapidity region and down to $p_{\rm T} = 0$. The inclusive Υ(1S) yield measured at forward rapidity by ALICE is more suppressed than that measured at mid-rapidity by CMS.

Two transport [22, 23, 46, 47] models and a dynamical [22, 46] model were considered. They both underestimate the measured suppression and fail to reproduce its rapidity dependence over the large range covered by ALICE ($2.5 < y < 4$) and CMS ($|y| < 2.4$). This might indicate that direct Υ(1S) are more suppressed than expected.

A better understanding of Υ production in heavy ion collisions requires a precise measurement of feed-down from higher mass bottomonia and CNM effects at forward rapidity. The ongoing study of Υ production in p–Pb collisions should help to gain further insight on the size of the CNM effects [49].

References

[1] E.V. Shuryak, Phys.Rept. 61 (1980) 71.

[2] M. Cheng et al., Phys.Rev. D81 (2010) 054504, 0911.2215.

[3] Wuppertal-Budapest Collaboration, S. Borsanyi et al., JHEP 1009 (2010) 073, 1005.3508.

[4] T. Matsui and H. Satz, Phys.Lett. B178 (1986) 416.

[5] N. Brambilla et al., Eur.Phys.J. C71 (2011) 1534, 1010.5827.

[6] NA50 Collaboration, B. Alessandro et al., Eur.Phys.J. C39 (2005) 335, hep-ex/0412036.

[7] NA60 Collaboration, R. Arnaldi et al., Phys.Rev.Lett. 99 (2007) 132302.

[8] PHENIX Collaboration, A. Adare et al., Phys.Rev.Lett. 98 (2007) 232301, nucl-ex/0611020.

[9] PHENIX Collaboration, A. Adare et al., Phys.Rev. C84 (2011) 054912, 1103.6269.

[10] STAR Collaboration, B. Abelev et al., Phys.Rev. C80 (2009) 041902, 0904.0439.

[11] P. Braun-Munzinger and J. Stachel, Phys.Lett. B490 (2000) 196, nucl-th/0007059.

[12] A. Andronic et al., Phys.Lett. B571 (2003) 36, nucl-th/0303036.

[13] L. Grandchamp, R. Rapp and G.E. Brown, Phys.Rev.Lett. 92 (2004) 212301, hep-ph/0306077.

[14] E. Bratkovskaya et al., Phys.Rev. C69 (2004) 054903, nucl-th/0402042.

[15] R. Thews and M. Mangano, Phys.Rev. C73 (2006) 014904, nucl-th/0505055.

[16] ALICE Collaboration, B. Abelev et al., Phys.Rev.Lett. 109 (2012) 072301, 1202.1383.

[17] ALICE Collaboration, B.B. Abelev et al., Phys.Lett. 743 (2014) 314, 1311.0214.

[18] S. Digal, P. Petreczky and H. Satz, Phys.Rev. D64 (2001) 094015, hep-ph/0106017.

[19] CMS Collaboration, S. Chatrchyan et al., Phys.Rev.Lett. 107 (2011) 052302, 1105.4894.

[20] CMS Collaboration, S. Chatrchyan et al., Phys.Rev.Lett. 109 (2012) 222301, 1208.2826.

[21] M. Strickland, AIP Conf.Proc. 1520 (2013) 179, 1207.5327.

[22] A. Emerick, X. Zhao and R. Rapp, Eur.Phys.J. A48 (2012) 72, 1111.6537.

[23] K. Zhou, N. Xu and P. Zhuang, (2013), 1309.7520.

[24] ALICE Collaboration, K. Aamodt et al., JINST 3 (2008) S08002.

[25] ALICE Collaboration, B. Abelev et al., Phys.Rev.Lett. 109 (2012) 252302, 1203.2436.

[26] ALICE Collaboration, B. Abelev et al., Phys.Rev. C88 (2013) 044909, 1301.4361.

[27] M.L. Miller et al., Ann.Rev.Nucl.Part.Sci. 57 (2007) 205, nucl-ex/0701025.

[28] ALICE Collaboration, K. Aamodt et al., Phys.Rev.Lett. 106 (2011) 032301, 1012.1657.

[29] V. Kumar, P. Shukla and R. Vogt, Phys.Rev. C86 (2012) 054907, 1205.3860.

[30] Particle Data Group, J. Beringer et al., Phys.Rev. D86 (2012) 010001.

[31] F. Bossu et al., (2011), 1103.2394.

[32] GEANT, GEANT-Detector description and simulation tool, CERN Program Library Long Write-up W5013, CERN Geneva.

[33] ALICE Collaboration, K. Aamodt et al., Phys.Lett. B704 (2011) 442, 1105.0380.

[34] D0 Collaboration, V. Abazov et al., Phys.Rev.Lett. 101 (2008) 182004, 0804.2799.

[35] CDF Collaboration, T. Aaltonen et al., Phys.Rev.Lett. 108 (2012) 151802, 1112.1591.

[36] CMS Collaboration, S. Chatrchyan et al., Phys.Rev.Lett. 110 (2013) 081802, 1209.2922.

[37] LHCb collaboration, R. Aaij et al., Eur.Phys.J. C74 (2014) 2835, 1402.2539.

[38] ALICE Collaboration, P. Khan, (2013), 1310.2565.

[39] LHCb Collaboration, R. Aaij et al., Eur.Phys.J. C72 (2012) 2025, 1202.6579.

[40] LHCb Collaboration, R. Aaij et al., JHEP 1211 (2012) 031, 1209.0282.

[41] CDF Collaboration, T. Affolder et al., Phys.Rev.Lett. 84 (2000) 2094, hep-ex/9910025.

[42] M. Strickland, Phys.Rev.Lett. 107 (2011) 132301, 1106.2571.

[43] M. Strickland and D. Bazow, Nucl.Phys. A879 (2012) 25, 1112.2761.

[44] J. Bjorken, Phys.Rev. D27 (1983) 140.

[45] L. Landau, Izv. Akad. Nauk SSSR, Ser. Fiz. .

[46] L. Grandchamp et al., Phys.Rev. C73 (2006) 064906, hep-ph/0507314.

[47] K. Zhou et al., Phys.Rev. C89 (2014) 054911, 1401.5845.

[48] K. Eskola, V. Kolhinen and C. Salgado, Eur.Phys.J. C9 (1999) 61, hep-ph/9807297.

[49] . B Abelev et al. [ALICE Collaboration], Y1S and Y2S production in p-Pb collisions at $\sqrt{s_{NN}} =$ 5.02 TeV, to be published.

[50] . J. E. Gaiser, Appendix-F, SLAC-R255.

[51] CDF Collaboration, D. Acosta et al., Phys.Rev.Lett. 88 (2002) 161802.

[52] D0 Collaboration, V. Abazov et al., Phys.Rev.Lett. 94 (2005) 232001, hep-ex/0502030.

[53] CMS Collaboration, S. Chatrchyan et al., JHEP 1205 (2012) 063, 1201.5069.

[54] CMS Collaboration, V. Khachatryan et al., Phys.Rev. D83 (2011) 112004, 1012.5545.

[55] T. Sjostrand, S. Mrenna and P.Z. Skands, JHEP 0605 (2006) 026, hep-ph/0603175.

[56] M. Gluck, J. Owens and E. Reya, Phys.Rev. D17 (1978) 2324.

[57] M. Cacciari et al., JHEP 1210 (2012) 137, 1205.6344.

[58] Quarkonium Working Group, N. Brambilla et al., (2004), hep-ph/0412158.

[59] G.T. Bodwin, E. Braaten and G.P. Lepage, Phys.Rev. D51 (1995) 1125, hep-ph/9407339.

[60] CTEQ Collaboration, H. Lai et al., Eur.Phys.J. C12 (2000) 375, hep-ph/9903282.

[61] J. Pumplin et al., JHEP 0207 (2002) 012, hep-ph/0201195.

A Extended Crystal Ball function

The Extended Crystal Ball function (CB2) derives from the Crystal Ball function [50] (CB). While the CB has only one power-law tail for low invariant masses, the CB2 has two power-law tails (one for higher masses, the other for lower ones). The CB2 is defined by the following equation:

$$f(x;N,\mu,\sigma,\alpha,n,\alpha',n') = N \cdot \begin{cases} e^{-\frac{(x-\mu)^2}{2\cdot\sigma^2}} & \text{if } -\alpha \leqslant \frac{x-\mu}{\sigma} < \alpha' \\ A \cdot \left(B - \frac{x-\mu}{\sigma}\right)^{-n} & \text{if } \frac{x-\mu}{\sigma} < -\alpha \\ C \cdot \left(D + \frac{x-\mu}{\sigma}\right)^{-n'} & \text{if } \frac{x-\mu}{\sigma} \geqslant \alpha' \end{cases}$$

$$A = \left(\frac{n}{|\alpha|}\right)^n \cdot e^{-\frac{|\alpha|^2}{2}}$$

$$B = \frac{n}{|\alpha|} - |\alpha|$$

$$C = \left(\frac{n'}{|\alpha'|}\right)^{n'} \cdot e^{-\frac{|\alpha'|^2}{2}}$$

$$D = \frac{n'}{|\alpha'|} - |\alpha'|$$

B Proton-proton reference cross-section in preliminary results

The method developed to obtained the pp reference cross section used in ALICE preliminary results [38] is explained in this appendix.

Few Υ(1S) cross section measurements in pp collisions at TeV energies exist and most of them refer to central rapidities [51–54]. Based on this data, the mid-rapidity differential cross section of Υ(1S) in pp collisions at $\sqrt{s} = 2.76$ TeV ($\mathrm{d}\sigma^{\mathrm{pp}}_{\Upsilon(1S)}/\mathrm{d}y|_{y=0}$) was estimated by means of an interpolation procedure (section B.1). The mid-rapidity cross section was then extrapolated to forward rapidities. For that purpose, y-differential distributions were predicted with different Pythia6.4 [55] tunes which were first selected according to their ability to reproduce the available forward and mid-rapidity data at $\sqrt{s} = 7$ TeV [39, 54] (see section B.2).

B.1 Interpolation of the Υ(1S) cross section at mid-rapidity

The measurements used for the interpolation of the Υ cross section at mid-rapidity are summarised in Table B.1.

Experiment	$\sqrt{s}$ (TeV)	$\mathrm{BR}\times\mathrm{d}\sigma^{\mathrm{pp}}_{\Upsilon(1S)}/\mathrm{d}y|_{y=0}$ (pb)	Range
CDF [51]	1.8	680 ± 15 (stat) ± 56 (syst)[a]	$\lvert y\rvert < 0.4$
D0 [52]	1.96	628 ± 16 (stat) ± 63 (syst)± 38 (lum)	$\lvert y\rvert < 0.6$
CMS [53]	2.76	921 ± 128 (stat) ± 157 (syst)± 55 (lum)	$\lvert y\rvert < 1.2$
CMS [54]	7	$2025\ ^{+284}_{-263}$ (stat + syst + lum)	$\lvert y\rvert < 0.4$

[a] From integration of the p_T-differential cross section quoted in [51].

Table B.1: Experimental results used for the interpolation of the Υ(1S) cross section at mid-rapidity. The cross section is corrected for BR, the branching ratio of Υ(1S) to dimuon.

Different functions were considered to describe the energy dependence of the cross section and to determine $\mathrm{d}\sigma^{\mathrm{pp}}_{\Upsilon(1S)}/\mathrm{d}y|_{y=0}$ at $\sqrt{s} = 2.76$ TeV. The statistical, systematic and luminosity uncertainties of each measurement were summed in quadrature in order to be used in the fit. As shown in Fig. B.1, the energy dependence of the cross section is well described by a power-law or a logarithmic function. Other functional forms were also tested, such as the sum of a logarithmic and a power-law function, or a three-parameter exponential function. The description of the data provided by such forms is less satisfactory and therefore they have been discarded, but we have checked that the obtained interpolation results are compatible within uncertainties with those obtained with the power-law and logarithmic function.

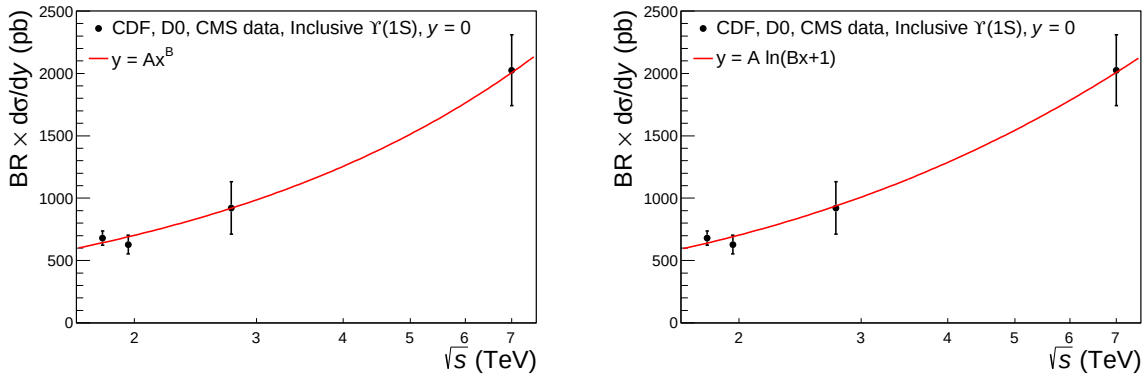

Fig. B.1: Energy dependence of the Υ cross section at mid-rapidity, with overlaid power-law (left) and logarithmic (right) fit.

Besides the purely empirical fit, a second option was considered for the interpolation. Models such as the Color Evaporation Model [56] predict that the quarkonium cross section is proportional to the bare quark pair production cross section. In such an approach, one can consider:

$$\frac{\mathrm{d}\sigma^{\mathrm{pp}}_{\Upsilon(1S)}}{\mathrm{d}y}(y,\sqrt{s}) = \alpha \frac{\mathrm{d}\sigma^{b\bar{b}}}{\mathrm{d}y}(y,\sqrt{s}) \tag{B.1}$$

where $\frac{\mathrm{d}\sigma^{b\bar{b}}}{\mathrm{d}y}$ is the $b\bar{b}$ production cross section calculated in perturbative QCD.

The available FONLL [57] predictions for the beauty cross section were used for the interpolation. They provide a central value and an uncertainty band obtained by varying the calculation parameters such as the quark mass or the factorisation scale. Three energy dependence curves were defined, corresponding to the central value and to the lower and upper edge of the uncertainty band. For each of the three curves, the α parameter was determined by fitting the ratio of data to FONLL to a constant value. Fig. B.2 shows the three FONLL predictions scaled by the α constant together with the measured cross sections. The model provides a good description of the data and can be used for the interpolation. The point at $\sqrt{s} = 2.76$ TeV provides the interpolated value.

The interpolation results at $\sqrt{s} = 2.76$ TeV obtained from the fit with the power-law and logarithmic functional forms and with the three FONLL curves were averaged. It was chosen to combine the largest fit uncertainty (6.2%) with the shape uncertainty defined as the difference between the average and the maximum and minimum of the obtained values (-1.1%+1.6%).

The interpolation at 2.76 TeV is strongly driven by the CDF and D0 measurements at 1.8 and 1.96 TeV. Although the two results are compatible within uncertainties, there is some tension between them, the data point at higher energy being below the data point at lower energy. In order to check the stability of the result, the procedure was repeated by alternatively excluding the CDF and D0 data point from the fit. A -4%(+6%) difference between the average value obtained with all data and that obtained by excluding the CDF (D0) data point was observed and added to the systematic uncertainties.

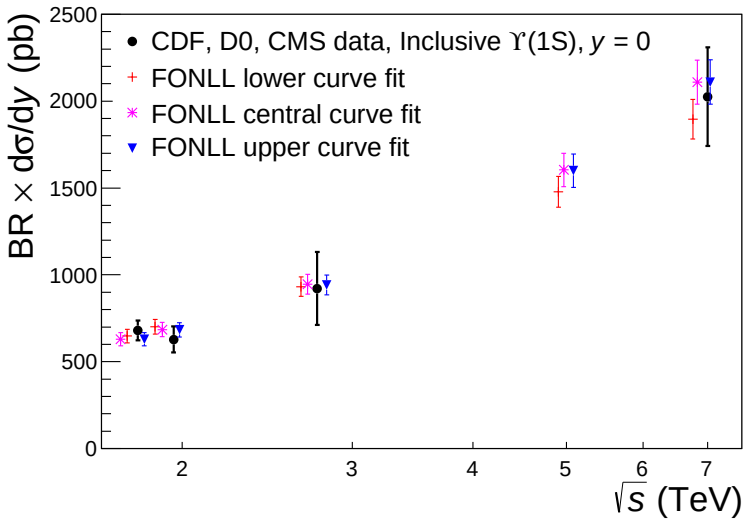

Fig. B.2: Energy dependence of the ϒ(1S) cross section at mid-rapidity, with overlaid FONLL predictions rescaled by the α parameter. The points corresponding to different predictions at the same energy are slightly shifted horizontally, for visibility.

The total uncertainty was obtained by summing in quadrature the three above-mentioned uncertainties[7] and amounts to 9%, yielding a final result of $\mathrm{d}\sigma^{\mathrm{pp}}_{\Upsilon(1S)}/\mathrm{d}y|_{y=0}$ ($\sqrt{s} = 2.76$ TeV) = (935 $\pm$ 82) pb.

B.2 Extrapolation to forward rapidity

The CMS Collaboration showed that Pythia6.4 [55] is able to reproduce the rapidity and the transverse momentum differential distributions of ϒ in pp collisions at $\sqrt{s} = 7$ TeV [54]. Taking advantage of this fact, the strategy to obtain the reference in the muon spectrometer rapidity range can be sketched as follows:

- Test the ϒ productions from Pythia6.4 with different tunes against 7 TeV data from LHC experiments.
- Use the tunes in agreement with 7 TeV data to generate ϒ events in pp collisions at $\sqrt{s} = 2.76$ TeV.
- Normalise the generated rapidity distribution at $\sqrt{s} = 2.76$ TeV to the mid-rapidity value estimated in section B.1.
- Obtain a forward rapidity estimate for ϒ cross section by combining the calculations relative to the different Pythia6.4 tunes.

The quarkonium production in Pythia6.4 can be performed following the prediction of two models: the Colour Singlet Model (CSM) [58] and the non-relativistic QCD (NRQCD) [59]. The Pythia interface in the ALICE simulation framework was customised in order to handle these two models for the bottomonium generation. With the NRQCD setting, it is possible to produce all the bottomonium states, while the CSM one just produces the ϒ(1S). Feed-down of ϒ(1S) from higher mass bottomonia is thus included only in the NRQCD setting.

In order to test the ability of Pythia6.4 to reproduce the rapidity distribution at $\sqrt{s} = 7$ TeV, the production of ϒ was performed using the two different models, with the different parton distribution function

[7] When dealing with asymmetric uncertainties, the largest between the positive and negative bar was taken.

(PDF) sets already available in the framework and different Pythia tunes. For each simulation, $80 \cdot 10^3$ bottomonium events were generated in the rapidity range $0 < y < 5.5$.

The Υ(1S) measurements in pp collisions at $\sqrt{s} = 7$ TeV from CMS [54] and LHCb [39] were chosen in order to test the Pythia6.4 calculations in the widest possible rapidity range. The statistical and systematic uncertainties quoted by the two experiments were summed in quadrature. The procedure for this test can be summarised as follow:

- The rapidity distributions ($\mathrm{d}N_\Upsilon/\mathrm{d}y$) of the generated Υ were binned as the experimental data.
- The ratios between the data and the simulation were fitted with a constant.
- The χ^2 of the fits was used as an estimation of how compatible the generated distributions are with the measured one.

The PDF sets considered for this test are: CTEQ5L [60], CTEQ6l [61], CTEQ6ll [61]. Pythia6.4 productions can be tuned in different ways. For this study, the sets of tunes considered are: *ATLAS-CSC*, *D6T*, *Perugia0*, *Z1*, *Z2*, *AMBT1*, *Schulz-Skands at 7TeV (s7)* and with a global fit (*Sglobal*). The detailed description of each setting can be found in the Pythia6.4 code. These tunes were used with the CTEQ6l PDF set. For the other PDF sets no specific tune was requested.

A $\chi^2/\mathrm{ndf} < 1.5$ was adopted as the limit for accepting the fit. In Fig. B.3, the simulated rapidity distributions that passed the test were plotted together with the experimental points for a visual comparison. Beforehand, the distributions were multiplied by the normalisation parameter provided by the constant fit.

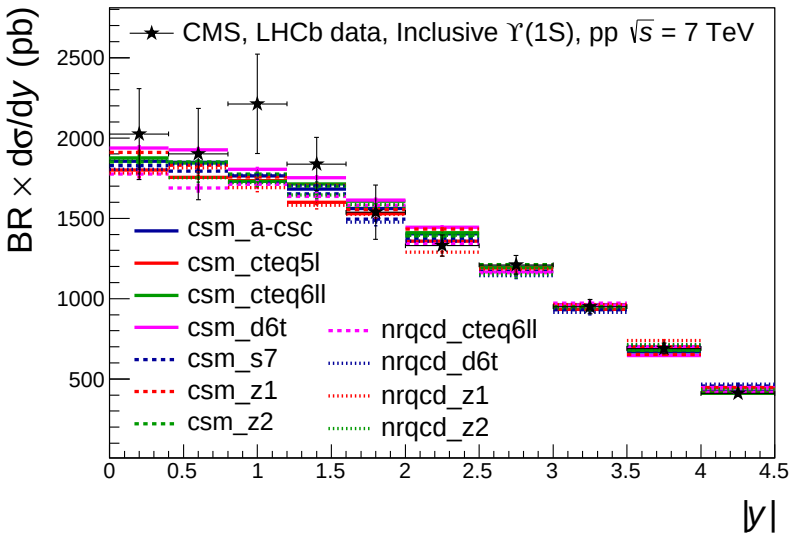

Fig. B.3: $\mathrm{d}\sigma^{\mathrm{pp}}_{\Upsilon(1\mathrm{S})}/\mathrm{d}y$ distributions obtained with Pythia6.4 productions. The shown distributions fit, with a $\chi^2/\mathrm{ndf} < 1.5$, those measured by CMS [54] and LHCb [39] experiments in pp collisions at $\sqrt{s} = 7$ TeV.

The extrapolation from mid to forward rapidity was performed by combining the results obtained simulating bottomonium states at $\sqrt{s} = 2.76$ TeV with the tunes that passed the test at 7 TeV as described previously. Rapidity distributions were obtained and normalised to the mid-rapidity interpolated cross section evaluated in section B.1. The $\mathrm{d}\sigma^{\mathrm{pp}}_{\Upsilon(1\mathrm{S})}/\mathrm{d}y$ in the muon spectrometer acceptance was computed for the rapidity intervals used in this analysis as the integral, in the considered bin, of the rapidity distribution divided by the bin width.

	$d\sigma^{pp}_{\Upsilon(1S)}/dy$ (nb)	Extr	Norm
$2.5 < y < 4$	12.5	$^{+1.9}_{-1.2}$	$\pm$ 1.1
$2.5 < y < 3.2$	17.2	$^{+1.6}_{-1.2}$	$\pm$ 1.5
$3.2 < y < 4$	8.4	$^{+2.1}_{-1.2}$	$\pm$ 0.7

Table B.2: Combined results for $d\sigma^{pp}_{\Upsilon(1S)}/dy$ in pp collisions at $\sqrt{s} = 2.76$ TeV at forward rapidity. The uncertainty on the normalisation (Norm) is quoted separately from the one related to the spread between the extrapolated values at forward rapidity (Extr).

In Table B.2, the results for the $d\sigma^{pp}_{\Upsilon(1S)}/dy$ at forward rapidity are summarised (after dividing by the $\Upsilon(1S) \to \mu^+\mu^-$ branching ratio BR $= 0.0248 \pm 0.0005$ [30]). They were obtained with an average over the values coming from the different Pythia6.4 Υ productions at 2.76 TeV. Two separate contributions of the systematic uncertainty are quoted. The first component (Extr) is associated to the extrapolation from mid to forward rapidity and results from the spread of calculations obtained with the different tunes that passed the test at 7 TeV. It is evaluated as the difference between the average value and the maximum and minimum values, while the second component (Norm) is related to the normalisation to the mid-rapidity point. The normalisation uncertainties are fully correlated with rapidity. The extrapolation uncertainties are taken uncorrelated with rapidity, since the spread observed among calculations is not the same from one range to an other. The statistical uncertainties (from the number of generated Υ) and the uncertainty on the branching ratio are negligible with respect to the systematic uncertainties.

In Fig. B.4, the obtained values at forward rapidity are plotted together with the CMS mid-rapidity [53] and the LHCb forward rapidity [37] data. The results of our interpolation are consistent with mid-rapidity data, while they underestimate the cross section measured at forward rapidity.

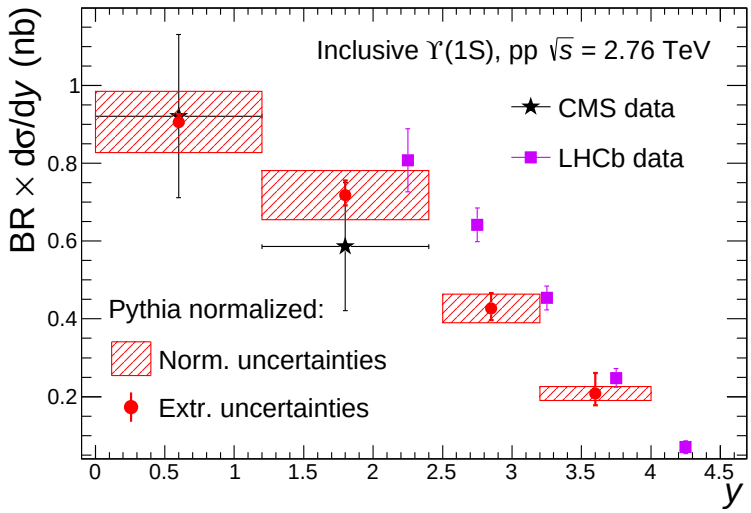

Fig. B.4: Combined Pythia6.4 BR·$d\sigma^{pp}_{\Upsilon(1S)}/dy$ for pp collisions at $\sqrt{s} = 2.76$ TeV, plotted together with CMS data points at mid-rapidity [53] and LHCb data points at forward rapidity [37]. Statistical and systematic uncertainties on data have been summed in quadrature. The error bars on the results of the Pythia normalization represent the uncorrelated uncertainty (Extr) while the boxes represent the correlated one (Norm). See the text for details.

C Acknowledgements

The ALICE collaboration would like to thank all its engineers and technicians for their invaluable contributions to the construction of the experiment and the CERN accelerator teams for the outstanding performance of the LHC complex.

The ALICE collaboration acknowledges the following funding agencies for their support in building and running the ALICE detector:
State Committee of Science, World Federation of Scientists (WFS) and Swiss Fonds Kidagan, Armenia, Conselho Nacional de Desenvolvimento Científico e Tecnológico (CNPq), Financiadora de Estudos e Projetos (FINEP), Fundação de Amparo à Pesquisa do Estado de São Paulo (FAPESP);
National Natural Science Foundation of China (NSFC), the Chinese Ministry of Education (CMOE) and the Ministry of Science and Technology of China (MSTC);
Ministry of Education and Youth of the Czech Republic;
Danish Natural Science Research Council, the Carlsberg Foundation and the Danish National Research Foundation;
The European Research Council under the European Community's Seventh Framework Programme;
Helsinki Institute of Physics and the Academy of Finland;
French CNRS-IN2P3, the 'Region Pays de Loire', 'Region Alsace', 'Region Auvergne' and CEA, France;
German BMBF and the Helmholtz Association;
General Secretariat for Research and Technology, Ministry of Development, Greece;
Hungarian OTKA and National Office for Research and Technology (NKTH);
Department of Atomic Energy and Department of Science and Technology of the Government of India;
Istituto Nazionale di Fisica Nucleare (INFN) and Centro Fermi - Museo Storico della Fisica e Centro Studi e Ricerche "Enrico Fermi", Italy;
MEXT Grant-in-Aid for Specially Promoted Research, Japan;
Joint Institute for Nuclear Research, Dubna;
National Research Foundation of Korea (NRF);
CONACYT, DGAPA, México, ALFA-EC and the EPLANET Program (European Particle Physics Latin American Network)
Stichting voor Fundamenteel Onderzoek der Materie (FOM) and the Nederlandse Organisatie voor Wetenschappelijk Onderzoek (NWO), Netherlands;
Research Council of Norway (NFR);
Polish Ministry of Science and Higher Education;
National Authority for Scientific Research - NASR (Autoritatea Naţională pentru Cercetare Ştiinţifică - ANCS);
Ministry of Education and Science of Russian Federation, Russian Academy of Sciences, Russian Federal Agency of Atomic Energy, Russian Federal Agency for Science and Innovations and The Russian Foundation for Basic Research;
Ministry of Education of Slovakia;
Department of Science and Technology, South Africa;
CIEMAT, EELA, Ministerio de Economía y Competitividad (MINECO) of Spain, Xunta de Galicia (Consellería de Educación), CEADEN, Cubaenergía, Cuba, and IAEA (International Atomic Energy Agency);
Swedish Research Council (VR) and Knut & Alice Wallenberg Foundation (KAW);
Ukraine Ministry of Education and Science;
United Kingdom Science and Technology Facilities Council (STFC);
The United States Department of Energy, the United States National Science Foundation, the State of Texas, and the State of Ohio.

D The ALICE Collaboration

B. Abelev[71] , J. Adam[37] , D. Adamová[79] , M.M. Aggarwal[83] , M. Agnello[90 ,107] , A. Agostinelli[26] , N. Agrawal[44] , Z. Ahammed[126] , N. Ahmad[18] , I. Ahmed[15] , S.U. Ahn[64] , S.A. Ahn[64] , I. Aimo[90 ,107] , S. Aiola[131] , M. Ajaz[15] , A. Akindinov[54] , S.N. Alam[126] , D. Aleksandrov[96] , B. Alessandro[107] , D. Alexandre[98] , A. Alici[12 ,101] ,

A. Alkin[3] , J. Alme[35] , T. Alt[39] , S. Altinpinar[17] , I. Altsybeev[125] , C. Alves Garcia Prado[115] , C. Andrei[74] , A. Andronic[93] , V. Anguelov[89] , J. Anielski[50] , T. Antičić[94] , F. Antinori[104] , P. Antonioli[101] , L. Aphecetche[109] , H. Appelshäuser[49] , S. Arcelli[26] , N. Armesto[16] , R. Arnaldi[107] , T. Aronsson[131] , I.C. Arsene[21 ,93] , M. Arslandok[49] , A. Augustinus[34] , R. Averbeck[93] , T.C. Awes[80] , M.D. Azmi[18 ,85] , M. Bach[39] , A. Badalà[103] , Y.W. Baek[40 ,66] , S. Bagnasco[107] , R. Bailhache[49] , R. Bala[86] , A. Baldisseri[14] , F. Baltasar Dos Santos Pedrosa[34] , R.C. Baral[57] , R. Barbera[27] , F. Barile[31] , G.G. Barnaföldi[130] , L.S. Barnby[98] , V. Barret[66] , J. Bartke[112] , M. Basile[26] , N. Bastid[66] , S. Basu[126] , B. Bathen[50] , G. Batigne[109] , B. Batyunya[62] , P.C. Batzing[21] , C. Baumann[49] , I.G. Bearden[76] , H. Beck[49] , C. Bedda[90] , N.K. Behera[44] , I. Belikov[51] , R. Bellwied[117] , E. Belmont-Moreno[60] , R. Belmont III[129] , V. Belyaev[72] , G. Bencedi[130] , S. Beole[25] , I. Berceanu[74] , A. Bercuci[74] , Y. Berdnikov[ii,81] , D. Berenyi[130] , M.E. Berger[88] , R.A. Bertens[53] , D. Berzano[25] , L. Betev[34] , A. Bhasin[86] , A.K. Bhati[83] , B. Bhattacharjee[41] , J. Bhom[122] , L. Bianchi[25] , N. Bianchi[68] , C. Bianchin[53] , J. Bielčík[37] , J. Bielčíková[79] , A. Bilandzic[76] , S. Bjelogrlic[53] , F. Blanco[10] , D. Blau[96] , C. Blume[49] , F. Bock[89 ,70] , A. Bogdanov[72] , H. Bøggild[76] , M. Bogolyubsky[108] , F.V. Böhmer[88] , L. Boldizsár[130] , M. Bombara[38] , J. Book[49] , H. Borel[14] , A. Borissov[92 ,129] , F. Bossú[61] , M. Botje[77] , E. Botta[25] , S. Böttger[48] , P. Braun-Munzinger[93] , M. Bregant[115] , T. Breitner[48] , T.A. Broker[49] , T.A. Browning[91] , M. Broz[37] , E. Bruna[107] , G.E. Bruno[31] , D. Budnikov[95] , H. Buesching[49] , S. Bufalino[107] , P. Buncic[34] , O. Busch[89] , Z. Buthelezi[61] , D. Caffarri[28 ,34] , X. Cai[7] , H. Caines[131] , L. Calero Diaz[68] , A. Caliva[53] , E. Calvo Villar[99] , P. Camerini[24] , F. Carena[34] , W. Carena[34] , J. Castillo Castellanos[14] , E.A.R. Casula[23] , V. Catanescu[74] , C. Cavicchioli[34] , C. Ceballos Sanchez[9] , J. Cepila[37] , P. Cerello[107] , B. Chang[118] , S. Chapeland[34] , J.L. Charvet[14] , S. Chattopadhyay[126] , S. Chattopadhyay[97] , M. Cherney[82] , C. Cheshkov[124] , B. Cheynis[124] , V. Chibante Barroso[34] , D.D. Chinellato[117 ,116] , P. Chochula[34] , M. Chojnacki[76] , S. Choudhury[126] , P. Christakoglou[77] , C.H. Christensen[76] , P. Christiansen[32] , T. Chujo[122] , S.U. Chung[92] , C. Cicalo[102] , L. Cifarelli[12 ,26] , F. Cindolo[101] , J. Cleymans[85] , F. Colamaria[31] , D. Colella[31] , A. Collu[23] , M. Colocci[26] , G. Conesa Balbastre[67] , Z. Conesa del Valle[47] , M.E. Connors[131] , J.G. Contreras[11] , T.M. Cormier[80 ,129] , Y. Corrales Morales[25] , P. Cortese[30] , I. Cortés Maldonado[2] , M.R. Cosentino[115] , F. Costa[34] , P. Crochet[66] , R. Cruz Albino[11] , E. Cuautle[59] , L. Cunqueiro[68 ,34] , A. Dainese[104] , R. Dang[7] , D. Das[97] , I. Das[47] , K. Das[97] , S. Das[4] , A. Dash[116] , S. Dash[44] , S. De[126] , H. Delagrange[109 ,i] , A. Deloff[73] , E. Dénes[130] , G. D'Erasmo[31] , A. De Caro[12 ,29] , G. de Cataldo[100] , J. de Cuveland[39] , A. De Falco[23] , D. De Gruttola[29 ,12] , N. De Marco[107] , S. De Pasquale[29] , R. de Rooij[53] , M.A. Diaz Corchero[10] , T. Dietel[50 ,85] , R. Divià[34] , D. Di Bari[31] , S. Di Liberto[105] , A. Di Mauro[34] , P. Di Nezza[68] , Ø. Djuvsland[17] , A. Dobrin[53] , T. Dobrowolski[73] , D. Domenicis Gimenez[115] , B. Dönigus[49] , O. Dordic[21] , S. Dørheim[88] , A.K. Dubey[126] , A. Dubla[53] , L. Ducroux[124] , P. Dupieux[66] , A.K. Dutta Majumdar[97] , R.J. Ehlers[131] , D. Elia[100] , H. Engel[48] , B. Erazmus[34 ,109] , H.A. Erdal[35] , D. Eschweiler[39] , B. Espagnon[47] , M. Esposito[34] , M. Estienne[109] , S. Esumi[122] , D. Evans[98] , S. Evdokimov[108] , D. Fabris[104] , J. Faivre[67] , D. Falchieri[26] , A. Fantoni[68] , M. Fasel[89] , D. Fehlker[17] , L. Feldkamp[50] , D. Felea[58] , A. Feliciello[107] , G. Feofilov[125] , J. Ferencei[79] , A. Fernández Téllez[2] , E.G. Ferreiro[16] , A. Ferretti[25] , A. Festanti[28] , J. Figiel[112] , S. Filchagin[95] , D. Finogeev[52] , F.M. Fionda[31 ,100] , E.M. Fiore[31] , E. Floratos[84] , M. Floris[34] , S. Foertsch[61] , P. Foka[93] , S. Fokin[96] , E. Fragiacomo[106] , A. Francescon[28 ,34] , U. Frankenfeld[93] , U. Fuchs[34] , C. Furget[67] , M. Fusco Girard[29] , J.J. Gaardhøje[76] , M. Gagliardi[25] , A.M. Gago[99] , M. Gallio[25] , D.R. Gangadharan[19 ,70] , P. Ganoti[84 ,80] , C. Garabatos[93] , E. Garcia-Solis[13] , C. Gargiulo[34] , I. Garishvili[71] , J. Gerhard[39] , M. Germain[109] , A. Gheata[34] , M. Gheata[58 ,34] , B. Ghidini[31] , P. Ghosh[126] , S.K. Ghosh[4] , P. Gianotti[68] , P. Giubellino[34] , E. Gladysz-Dziadus[112] , P. Glässel[89] , A. Gomez Ramirez[48] , P. González-Zamora[10] , S. Gorbunov[39] , L. Görlich[112] , S. Gotovac[111] , L.K. Graczykowski[128] , A. Grelli[53] , A. Grigoras[34] , C. Grigoras[34] , V. Grigoriev[72] , A. Grigoryan[1] , S. Grigoryan[62] , B. Grinyov[3] , N. Grion[106] , J.F. Grosse-Oetringhaus[34] , J.-Y. Grossiord[124] , R. Grosso[34] , F. Guber[52] , R. Guernane[67] , B. Guerzoni[26] , M. Guilbaud[124] , K. Gulbrandsen[76] , H. Gulkanyan[1] , M. Gumbo[85] , T. Gunji[121] , A. Gupta[86] , R. Gupta[86] , K. H. Khan[15] , R. Haake[50] , Ø. Haaland[17] , C. Hadjidakis[47] , M. Haiduc[58] , H. Hamagaki[121] , G. Hamar[130] , L.D. Hanratty[98] , A. Hansen[76] , J.W. Harris[131] , H. Hartmann[39] , A. Harton[13] , D. Hatzifotiadou[101] , S. Hayashi[121] , S.T. Heckel[49] , M. Heide[50] , H. Helstrup[35] , A. Herghelegiu[74] , G. Herrera Corral[11] , B.A. Hess[33] , K.F. Hetland[35] , B. Hippolyte[51] , J. Hladky[56] , P. Hristov[34] , M. Huang[17] , T.J. Humanic[19] , D. Hutter[39] , D.S. Hwang[20] , R. Ilkaev[95] , I. Ilkiv[73] , M. Inaba[122] , G.M. Innocenti[25] , C. Ionita[34] , M. Ippolitov[96] , M. Irfan[18] , M. Ivanov[93] , V. Ivanov[81] , A. Jachołkowski[27] , P.M. Jacobs[70] , C. Jahnke[115] , H.J. Jang[64] , M.A. Janik[128] , P.H.S.Y. Jayarathna[117] , S. Jena[117] , R.T. Jimenez Bustamante[59] , P.G. Jones[98] , H. Jung[40] , A. Jusko[98] , S. Kalcher[39] , P. Kalinak[55] , A. Kalweit[34] , J. Kamin[49] , J.H. Kang[132] , V. Kaplin[72] , S. Kar[126] , A. Karasu Uysal[65] , O. Karavichev[52] , T. Karavicheva[52] , E. Karpechev[52] , U. Kebschull[48] , R. Keidel[133] , D.L.D. Keijdener[53] , M.M. Khan[iii,18] , P. Khan[97] , S.A. Khan[126] , A. Khanzadeev[81] , Y. Kharlov[108] , B. Kileng[35] , B. Kim[132] , D.W. Kim[64 ,40] , D.J. Kim[118] , J.S. Kim[40] , M. Kim[40] , M. Kim[132] , S. Kim[20] , T. Kim[132] ,

S. Kirsch[39] , I. Kisel[39] , S. Kiselev[54] , A. Kisiel[128] , G. Kiss[130] , J.L. Klay[6] , J. Klein[89] , C. Klein-Bösing[50] , A. Kluge[34] , M.L. Knichel[93,89] , A.G. Knospe[113] , C. Kobdaj[110,34] , M. Kofarago[34] , M.K. Köhler[93] , T. Kollegger[39] , A. Kolojvari[125] , V. Kondratiev[125] , N. Kondratyeva[72] , A. Konevskikh[52] , V. Kovalenko[125] , M. Kowalski[34,112] , S. Kox[67] , G. Koyithatta Meethaleveedu[44] , J. Kral[118] , I. Králik[55] , F. Kramer[49] , A. Kravčáková[38] , M. Krelina[37] , M. Kretz[39] , M. Krivda[55,98] , F. Krizek[79] , M. Krzewicki[93] , V. Kučera[79] , Y. Kucheriaev[96,i], T. Kugathasan[34] , C. Kuhn[51] , P.G. Kuijer[77] , I. Kulakov[49,39] , J. Kumar[44] , P. Kurashvili[73] , A. Kurepin[52] , A.B. Kurepin[52] , A. Kuryakin[95] , S. Kushpil[79] , M.J. Kweon[46,89] , Y. Kwon[132] , P. Ladron de Guevara[59] , C. Lagana Fernandes[115] , I. Lakomov[47] , R. Langoy[127] , C. Lara[48] , A. Lardeux[109] , A. Lattuca[25] , S.L. La Pointe[53,107] , P. La Rocca[27] , R. Lea[24] , G.R. Lee[98] , I. Legrand[34] , J. Lehnert[49] , R.C. Lemmon[78] , V. Lenti[100] , E. Leogrande[53] , M. Leoncino[25] , I. León Monzón[114] , P. Lévai[130] , S. Li[7,66] , J. Lien[127] , R. Lietava[98] , S. Lindal[21] , V. Lindenstruth[39] , C. Lippmann[93] , M.A. Lisa[19] , H.M. Ljunggren[32] , D.F. Lodato[53] , P.I. Loenne[17] , V.R. Loggins[129] , V. Loginov[72] , D. Lohner[89] , C. Loizides[70] , X. Lopez[66] , E. López Torres[9] , X.-G. Lu[89] , P. Luettig[49] , M. Lunardon[28] , G. Luparello[53] , C. Luzzi[34] , R. Ma[131] , A. Maevskaya[52] , M. Mager[34] , D.P. Mahapatra[57] , S.M. Mahmood[21] , A. Maire[51,89] , R.D. Majka[131] , M. Malaev[81] , I. Maldonado Cervantes[59] , L. Malinina[iv,62] , D. Mal'Kevich[54] , P. Malzacher[93] , A. Mamonov[95] , L. Manceau[107] , V. Manko[96] , F. Manso[66] , V. Manzari[34,100] , M. Marchisone[66,25] , J. Mareš[56] , G.V. Margagliotti[24] , A. Margotti[101] , A. Marín[93] , C. Markert[34,113] , M. Marquard[49] , I. Martashvili[120] , N.A. Martin[93] , P. Martinengo[34] , M.I. Martínez[2] , G. Martínez García[109] , J. Martin Blanco[109] , Y. Martynov[3] , A. Mas[109] , S. Masciocchi[93] , M. Masera[25] , A. Masoni[102] , L. Massacrier[109] , A. Mastroserio[31] , A. Matyja[112] , C. Mayer[112] , J. Mazer[120] , M.A. Mazzoni[105] , F. Meddi[22] , A. Menchaca-Rocha[60] , E. Meninno[29] , J. Mercado Pérez[89] , M. Meres[36] , Y. Miake[122] , K. Mikhaylov[54,62] , L. Milano[34] , J. Milosevic[v,21] , A. Mischke[53] , A.N. Mishra[45] , D. Miśkowiec[93] , J. Mitra[126] , C.M. Mitu[58] , J. Mlynarz[129] , N. Mohammadi[53] , B. Mohanty[126,75] , L. Molnar[51] , L. Montaño Zetina[11] , E. Montes[10] , M. Morando[28] , D.A. Moreira De Godoy[115] , S. Moretto[28] , A. Morsch[34] , V. Muccifora[68] , E. Mudnic[111] , D. Mühlheim[50] , S. Muhuri[126] , M. Mukherjee[126] , H. Müller[34] , M.G. Munhoz[115] , S. Murray[85] , L. Musa[34] , J. Musinsky[55] , B.K. Nandi[44] , R. Nania[101] , E. Nappi[100] , C. Nattrass[120] , K. Nayak[75] , T.K. Nayak[126] , S. Nazarenko[95] , A. Nedosekin[54] , M. Nicassio[93] , M. Niculescu[34,58] , B.S. Nielsen[76] , S. Nikolaev[96] , S. Nikulin[96] , V. Nikulin[81] , B.S. Nilsen[82] , F. Noferini[12,101] , P. Nomokonov[62] , G. Nooren[53] , J. Norman[119] , A. Nyanin[96] , J. Nystrand[17] , H. Oeschler[89] , S. Oh[131] , S.K. Oh[vi,63,40] , A. Okatan[65] , L. Olah[130] , J. Oleniacz[128] , A.C. Oliveira Da Silva[115] , J. Onderwaater[93] , C. Oppedisano[107] , A. Ortiz Velasquez[59,32] , A. Oskarsson[32] , J. Otwinowski[93] , K. Oyama[89] , P. Sahoo[45] , Y. Pachmayer[89] , M. Pachr[37] , P. Pagano[29] , G. Paić[59] , F. Painke[39] , C. Pajares[16] , S.K. Pal[126] , A. Palmeri[103] , D. Pant[44] , V. Papikyan[1] , G.S. Pappalardo[103] , P. Pareek[45] , W.J. Park[93] , S. Parmar[83] , A. Passfeld[50] , D.I. Patalakha[108] , V. Paticchio[100] , B. Paul[97] , T. Pawlak[128] , T. Peitzmann[53] , H. Pereira Da Costa[14] , E. Pereira De Oliveira Filho[115] , D. Peresunko[96] , C.E. Pérez Lara[77] , A. Pesci[101] , Y. Pestov[5] , V. Petráček[37] , M. Petran[37] , M. Petris[74] , M. Petrovici[74] , C. Petta[27] , S. Piano[106] , M. Pikna[36] , P. Pillot[109] , O. Pinazza[34,101] , L. Pinsky[117] , D.B. Piyarathna[117] , M. Płoskoń[70] , M. Planinic[123,94] , J. Pluta[128] , S. Pochybova[130] , P.L.M. Podesta-Lerma[114] , M.G. Poghosyan[34,82] , E.H.O. Pohjoisaho[42] , B. Polichtchouk[108] , N. Poljak[123,94] , A. Pop[74] , S. Porteboeuf-Houssais[66] , J. Porter[70] , B. Potukuchi[86] , S.K. Prasad[4,129] , R. Preghenella[101,12] , F. Prino[107] , C.A. Pruneau[129] , I. Pshenichnov[52] , M. Puccio[107] , G. Puddu[23] , P. Pujahari[129] , V. Punin[95] , J. Putschke[129] , H. Qvigstad[21] , A. Rachevski[106] , S. Raha[4] , J. Rak[118] , A. Rakotozafindrabe[14] , L. Ramello[30] , R. Raniwala[87] , S. Raniwala[87] , S.S. Räsänen[42] , B.T. Rascanu[49] , D. Rathee[83] , A.W. Rauf[15] , V. Razazi[23] , K.F. Read[120] , J.S. Real[67] , K. Redlich[vii,73] , R.J. Reed[131,129] , A. Rehman[17] , P. Reichelt[49] , M. Reicher[53] , F. Reidt[34,89] , R. Renfordt[49] , A.R. Reolon[68] , A. Reshetin[52] , F. Rettig[39] , J.-P. Revol[34] , K. Reygers[89] , V. Riabov[81] , R.A. Ricci[69] , T. Richert[32] , M. Richter[21] , P. Riedler[34] , W. Riegler[34] , F. Riggi[27] , A. Rivetti[107] , E. Rocco[53] , M. Rodríguez Cahuantzi[2] , A. Rodriguez Manso[77] , K. Røed[21] , E. Rogochaya[62] , S. Rohni[86] , D. Rohr[39] , D. Röhrich[17] , R. Romita[78,119] , F. Ronchetti[68] , L. Ronflette[109] , P. Rosnet[66] , A. Rossi[34] , F. Roukoutakis[84] , A. Roy[45] , C. Roy[51] , P. Roy[97] , A.J. Rubio Montero[10] , R. Rui[24] , R. Russo[25] , E. Ryabinkin[96] , Y. Ryabov[81] , A. Rybicki[112] , S. Sadovsky[108] , K. Šafařík[34] , B. Sahlmuller[49] , R. Sahoo[45] , P.K. Sahu[57] , J. Saini[126] , S. Sakai[68,70] , C.A. Salgado[16] , J. Salzwedel[19] , S. Sambyal[86] , V. Samsonov[81] , X. Sanchez Castro[51] , F.J. Sánchez Rodríguez[114] , L. Šándor[55] , A. Sandoval[60] , M. Sano[122] , G. Santagati[27] , D. Sarkar[126] , E. Scapparone[101] , F. Scarlassara[28] , R.P. Scharenberg[91] , C. Schiaua[74] , R. Schicker[89] , C. Schmidt[93] , H.R. Schmidt[33] , S. Schuchmann[49] , J. Schukraft[34] , M. Schulc[37] , T. Schuster[131] , Y. Schutz[109,34] , K. Schwarz[93] , K. Schweda[93] , G. Scioli[26] , E. Scomparin[107] , R. Scott[120] , G. Segato[28] , J.E. Seger[82] , I. Selyuzhenkov[93] , J. Seo[92] , E. Serradilla[10,60] , A. Sevcenco[58] , A. Shabetai[109] , G. Shabratova[62] , R. Shahoyan[34] , A. Shangaraev[108] , N. Sharma[120,57] , S. Sharma[86] , K. Shigaki[43] , K. Shtejer[25] , Y. Sibiriak[96] , S. Siddhanta[102] , T. Siemiarczuk[73] , D. Silvermyr[80] , C. Silvestre[67] , G. Simatovic[123] , R. Singaraju[126] , R. Singh[86] , S. Singha[75,126] , V. Singhal[126] , B.C. Sinha[126] ,

T. Sinha[97] , B. Sitar[36] , M. Sitta[30] , T.B. Skaali[21] , K. Skjerdal[17] , N. Smirnov[131] , R.J.M. Snellings[53] , C. Søgaard[32] , R. Soltz[71] , J. Song[92] , M. Song[132] , F. Soramel[28] , S. Sorensen[120] , M. Spacek[37] , I. Sputowska[112] , M. Spyropoulou-Stassinaki[84] , B.K. Srivastava[91] , J. Stachel[89] , I. Stan[58] , G. Stefanek[73] , M. Steinpreis[19] , E. Stenlund[32] , G. Steyn[61] , J.H. Stiller[89] , D. Stocco[109] , M. Stolpovskiy[108] , P. Strmen[36] , A.A.P. Suaide[115] , T. Sugitate[43] , C. Suire[47] , M. Suleymanov[15] , R. Sultanov[54] , M. Šumbera[79] , T. Susa[94] , T.J.M. Symons[70] , A. Szabo[36] , A. Szanto de Toledo[115] , I. Szarka[36] , A. Szczepankiewicz[34] , M. Szymanski[128] , J. Takahashi[116] , M.A. Tangaro[31] , J.D. Tapia Takaki[i,viii,47] , A. Tarantola Peloni[49] , A. Tarazona Martinez[34] , M.G. Tarzila[74] , A. Tauro[34] , G. Tejeda Muñoz[2] , A. Telesca[34] , C. Terrevoli[23] , J. Thäder[93] , D. Thomas[53] , R. Tieulent[124] , A.R. Timmins[117] , A. Toia[104,49] , W.H. Trzaska[118] , T. Tsuji[121] , A. Tumkin[95] , R. Turrisi[104] , T.S. Tveter[21] , K. Ullaland[17] , A. Uras[124] , G.L. Usai[23] , M. Vajzer[79] , M. Vala[55,62] , L. Valencia Palomo[66] , S. Vallero[25,89] , P. Vande Vyvre[34] , L. Vannucci[69] , J. Van Der Maarel[53] , J.W. Van Hoorne[34] , M. van Leeuwen[53] , A. Vargas[2] , M. Vargyas[118] , R. Varma[44] , M. Vasileiou[84] , A. Vasiliev[96] , V. Vechernin[125] , M. Veldhoen[53] , A. Velure[17] , M. Venaruzzo[24,69] , E. Vercellin[25] , S. Vergara Limón[2] , R. Vernet[8] , L. Vickovic[111] , G. Viesti[28] , J. Viinikainen[118] , Z. Vilakazi[61] , O. Villalobos Baillie[98] , A. Vinogradov[96] , L. Vinogradov[125] , Y. Vinogradov[95] , T. Virgili[29] , Y.P. Viyogi[126] , A. Vodopyanov[62] , M.A. Völkl[89] , K. Voloshin[54] , S.A. Voloshin[129] , G. Volpe[34] , B. von Haller[34] , I. Vorobyev[125] , D. Vranic[93,34] , J. Vrláková[38] , B. Vulpescu[66] , A. Vyushin[95] , B. Wagner[17] , J. Wagner[93] , V. Wagner[37] , M. Wang[7,109] , Y. Wang[89] , D. Watanabe[122] , M. Weber[34,117] , S.G. Weber[93] , J.P. Wessels[50] , U. Westerhoff[50] , J. Wiechula[33] , J. Wikne[21] , M. Wilde[50] , G. Wilk[73] , J. Wilkinson[89] , M.C.S. Williams[101] , B. Windelband[89] , M. Winn[89] , C.G. Yaldo[129] , Y. Yamaguchi[121] , H. Yang[53] , P. Yang[7] , S. Yang[17] , S. Yano[43] , S. Yasnopolskiy[96] , J. Yi[92] , Z. Yin[7] , I.-K. Yoo[92] , I. Yushmanov[96] , V. Zaccolo[76] , C. Zach[37] , A. Zaman[15] , C. Zampolli[101] , S. Zaporozhets[62] , A. Zarochentsev[125] , P. Závada[56] , N. Zaviyalov[95] , H. Zbroszczyk[128] , I.S. Zgura[58] , M. Zhalov[81] , H. Zhang[7] , X. Zhang[70,7] , Y. Zhang[7] , C. Zhao[21] , N. Zhigareva[54] , D. Zhou[7] , F. Zhou[7] , Y. Zhou[53] , Zhou, Zhuo[17] , H. Zhu[7] , J. Zhu[109,7] , X. Zhu[7] , A. Zichichi[26,12] , A. Zimmermann[89] , M.B. Zimmermann[34,50] , G. Zinovjev[3] , Y. Zoccarato[124] , M. Zyzak[49,39]

Affiliation notes

[i] Deceased
[ii] Also at: St. Petersburg State Polytechnical University
[iii] Also at: Department of Applied Physics, Aligarh Muslim University, Aligarh, India
[iv] Also at: M.V. Lomonosov Moscow State University, D.V. Skobeltsyn Institute of Nuclear Physics, Moscow, Russia
[v] Also at: University of Belgrade, Faculty of Physics and ”Vinča” Institute of Nuclear Sciences, Belgrade, Serbia
[vi] Permanent Address: Permanent Address: Konkuk University, Seoul, Korea
[vii] Also at: Institute of Theoretical Physics, University of Wroclaw, Wroclaw, Poland
[viii] Also at: University of Kansas, Lawrence, KS, United States

Collaboration Institutes

[1] A.I. Alikhanyan National Science Laboratory (Yerevan Physics Institute) Foundation, Yerevan, Armenia
[2] Benemérita Universidad Autónoma de Puebla, Puebla, Mexico
[3] Bogolyubov Institute for Theoretical Physics, Kiev, Ukraine
[4] Bose Institute, Department of Physics and Centre for Astroparticle Physics and Space Science (CAPSS), Kolkata, India
[5] Budker Institute for Nuclear Physics, Novosibirsk, Russia
[6] California Polytechnic State University, San Luis Obispo, CA, United States
[7] Central China Normal University, Wuhan, China
[8] Centre de Calcul de l’IN2P3, Villeurbanne, France
[9] Centro de Aplicaciones Tecnológicas y Desarrollo Nuclear (CEADEN), Havana, Cuba
[10] Centro de Investigaciones Energéticas Medioambientales y Tecnológicas (CIEMAT), Madrid, Spain
[11] Centro de Investigación y de Estudios Avanzados (CINVESTAV), Mexico City and Mérida, Mexico
[12] Centro Fermi - Museo Storico della Fisica e Centro Studi e Ricerche “Enrico Fermi”, Rome, Italy
[13] Chicago State University, Chicago, USA
[14] Commissariat à l’Energie Atomique, IRFU, Saclay, France
[15] COMSATS Institute of Information Technology (CIIT), Islamabad, Pakistan

[16] Departamento de Física de Partículas and IGFAE, Universidad de Santiago de Compostela, Santiago de Compostela, Spain
[17] Department of Physics and Technology, University of Bergen, Bergen, Norway
[18] Department of Physics, Aligarh Muslim University, Aligarh, India
[19] Department of Physics, Ohio State University, Columbus, OH, United States
[20] Department of Physics, Sejong University, Seoul, South Korea
[21] Department of Physics, University of Oslo, Oslo, Norway
[22] Dipartimento di Fisica dell'Università 'La Sapienza' and Sezione INFN Rome, Italy
[23] Dipartimento di Fisica dell'Università and Sezione INFN, Cagliari, Italy
[24] Dipartimento di Fisica dell'Università and Sezione INFN, Trieste, Italy
[25] Dipartimento di Fisica dell'Università and Sezione INFN, Turin, Italy
[26] Dipartimento di Fisica e Astronomia dell'Università and Sezione INFN, Bologna, Italy
[27] Dipartimento di Fisica e Astronomia dell'Università and Sezione INFN, Catania, Italy
[28] Dipartimento di Fisica e Astronomia dell'Università and Sezione INFN, Padova, Italy
[29] Dipartimento di Fisica 'E.R. Caianiello' dell'Università and Gruppo Collegato INFN, Salerno, Italy
[30] Dipartimento di Scienze e Innovazione Tecnologica dell'Università del Piemonte Orientale and Gruppo Collegato INFN, Alessandria, Italy
[31] Dipartimento Interateneo di Fisica 'M. Merlin' and Sezione INFN, Bari, Italy
[32] Division of Experimental High Energy Physics, University of Lund, Lund, Sweden
[33] Eberhard Karls Universität Tübingen, Tübingen, Germany
[34] European Organization for Nuclear Research (CERN), Geneva, Switzerland
[35] Faculty of Engineering, Bergen University College, Bergen, Norway
[36] Faculty of Mathematics, Physics and Informatics, Comenius University, Bratislava, Slovakia
[37] Faculty of Nuclear Sciences and Physical Engineering, Czech Technical University in Prague, Prague, Czech Republic
[38] Faculty of Science, P.J. Šafárik University, Košice, Slovakia
[39] Frankfurt Institute for Advanced Studies, Johann Wolfgang Goethe-Universität Frankfurt, Frankfurt, Germany
[40] Gangneung-Wonju National University, Gangneung, South Korea
[41] Gauhati University, Department of Physics, Guwahati, India
[42] Helsinki Institute of Physics (HIP), Helsinki, Finland
[43] Hiroshima University, Hiroshima, Japan
[44] Indian Institute of Technology Bombay (IIT), Mumbai, India
[45] Indian Institute of Technology Indore, Indore (IITI), India
[46] Inha University, Incheon, South Korea
[47] Institut de Physique Nucléaire d'Orsay (IPNO), Université Paris-Sud, CNRS-IN2P3, Orsay, France
[48] Institut für Informatik, Johann Wolfgang Goethe-Universität Frankfurt, Frankfurt, Germany
[49] Institut für Kernphysik, Johann Wolfgang Goethe-Universität Frankfurt, Frankfurt, Germany
[50] Institut für Kernphysik, Westfälische Wilhelms-Universität Münster, Münster, Germany
[51] Institut Pluridisciplinaire Hubert Curien (IPHC), Université de Strasbourg, CNRS-IN2P3, Strasbourg, France
[52] Institute for Nuclear Research, Academy of Sciences, Moscow, Russia
[53] Institute for Subatomic Physics of Utrecht University, Utrecht, Netherlands
[54] Institute for Theoretical and Experimental Physics, Moscow, Russia
[55] Institute of Experimental Physics, Slovak Academy of Sciences, Košice, Slovakia
[56] Institute of Physics, Academy of Sciences of the Czech Republic, Prague, Czech Republic
[57] Institute of Physics, Bhubaneswar, India
[58] Institute of Space Science (ISS), Bucharest, Romania
[59] Instituto de Ciencias Nucleares, Universidad Nacional Autónoma de México, Mexico City, Mexico
[60] Instituto de Física, Universidad Nacional Autónoma de México, Mexico City, Mexico
[61] iThemba LABS, National Research Foundation, Somerset West, South Africa
[62] Joint Institute for Nuclear Research (JINR), Dubna, Russia
[63] Konkuk University, Seoul, South Korea
[64] Korea Institute of Science and Technology Information, Daejeon, South Korea
[65] KTO Karatay University, Konya, Turkey
[66] Laboratoire de Physique Corpusculaire (LPC), Clermont Université, Université Blaise Pascal,

CNRS–IN2P3, Clermont-Ferrand, France
[67] Laboratoire de Physique Subatomique et de Cosmologie, Université Grenoble-Alpes, CNRS-IN2P3, Grenoble, France
[68] Laboratori Nazionali di Frascati, INFN, Frascati, Italy
[69] Laboratori Nazionali di Legnaro, INFN, Legnaro, Italy
[70] Lawrence Berkeley National Laboratory, Berkeley, CA, United States
[71] Lawrence Livermore National Laboratory, Livermore, CA, United States
[72] Moscow Engineering Physics Institute, Moscow, Russia
[73] National Centre for Nuclear Studies, Warsaw, Poland
[74] National Institute for Physics and Nuclear Engineering, Bucharest, Romania
[75] National Institute of Science Education and Research, Bhubaneswar, India
[76] Niels Bohr Institute, University of Copenhagen, Copenhagen, Denmark
[77] Nikhef, National Institute for Subatomic Physics, Amsterdam, Netherlands
[78] Nuclear Physics Group, STFC Daresbury Laboratory, Daresbury, United Kingdom
[79] Nuclear Physics Institute, Academy of Sciences of the Czech Republic, Řež u Prahy, Czech Republic
[80] Oak Ridge National Laboratory, Oak Ridge, TN, United States
[81] Petersburg Nuclear Physics Institute, Gatchina, Russia
[82] Physics Department, Creighton University, Omaha, NE, United States
[83] Physics Department, Panjab University, Chandigarh, India
[84] Physics Department, University of Athens, Athens, Greece
[85] Physics Department, University of Cape Town, Cape Town, South Africa
[86] Physics Department, University of Jammu, Jammu, India
[87] Physics Department, University of Rajasthan, Jaipur, India
[88] Physik Department, Technische Universität München, Munich, Germany
[89] Physikalisches Institut, Ruprecht-Karls-Universität Heidelberg, Heidelberg, Germany
[90] Politecnico di Torino, Turin, Italy
[91] Purdue University, West Lafayette, IN, United States
[92] Pusan National University, Pusan, South Korea
[93] Research Division and ExtreMe Matter Institute EMMI, GSI Helmholtzzentrum für Schwerionenforschung, Darmstadt, Germany
[94] Rudjer Bošković Institute, Zagreb, Croatia
[95] Russian Federal Nuclear Center (VNIIEF), Sarov, Russia
[96] Russian Research Centre Kurchatov Institute, Moscow, Russia
[97] Saha Institute of Nuclear Physics, Kolkata, India
[98] School of Physics and Astronomy, University of Birmingham, Birmingham, United Kingdom
[99] Sección Física, Departamento de Ciencias, Pontificia Universidad Católica del Perú, Lima, Peru
[100] Sezione INFN, Bari, Italy
[101] Sezione INFN, Bologna, Italy
[102] Sezione INFN, Cagliari, Italy
[103] Sezione INFN, Catania, Italy
[104] Sezione INFN, Padova, Italy
[105] Sezione INFN, Rome, Italy
[106] Sezione INFN, Trieste, Italy
[107] Sezione INFN, Turin, Italy
[108] SSC IHEP of NRC Kurchatov institute, Protvino, Russia
[109] SUBATECH, Ecole des Mines de Nantes, Université de Nantes, CNRS-IN2P3, Nantes, France
[110] Suranaree University of Technology, Nakhon Ratchasima, Thailand
[111] Technical University of Split FESB, Split, Croatia
[112] The Henryk Niewodniczanski Institute of Nuclear Physics, Polish Academy of Sciences, Cracow, Poland
[113] The University of Texas at Austin, Physics Department, Austin, TX, USA
[114] Universidad Autónoma de Sinaloa, Culiacán, Mexico
[115] Universidade de São Paulo (USP), São Paulo, Brazil
[116] Universidade Estadual de Campinas (UNICAMP), Campinas, Brazil
[117] University of Houston, Houston, TX, United States
[118] University of Jyväskylä, Jyväskylä, Finland
[119] University of Liverpool, Liverpool, United Kingdom

[120] University of Tennessee, Knoxville, TN, United States
[121] University of Tokyo, Tokyo, Japan
[122] University of Tsukuba, Tsukuba, Japan
[123] University of Zagreb, Zagreb, Croatia
[124] Université de Lyon, Université Lyon 1, CNRS/IN2P3, IPN-Lyon, Villeurbanne, France
[125] V. Fock Institute for Physics, St. Petersburg State University, St. Petersburg, Russia
[126] Variable Energy Cyclotron Centre, Kolkata, India
[127] Vestfold University College, Tonsberg, Norway
[128] Warsaw University of Technology, Warsaw, Poland
[129] Wayne State University, Detroit, MI, United States
[130] Wigner Research Centre for Physics, Hungarian Academy of Sciences, Budapest, Hungary
[131] Yale University, New Haven, CT, United States
[132] Yonsei University, Seoul, South Korea
[133] Zentrum für Technologietransfer und Telekommunikation (ZTT), Fachhochschule Worms, Worms, Germany